

FINAL REPORT

PROJECT B-905

DETERMINATION OF DYNAMIC FLUID PRESSURES

By: Helmut F. Bauer

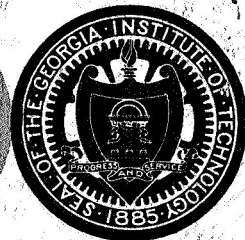
CR-102261

Contract NAS8-11389

FACILITY FORM 602	N69-80142	
	(ACCESSION NUMBER)	(THRU)
	56	NONE
	(PAGES)	(CODE)
	CR-102261	
	(NASA CR OR TMX OR AD NUMBER)	(CATEGORY)

Prepared for  
George C. Marshall Space Flight Center  
National Aeronautics and Space Administration  
Huntsville, Alabama

May 31, 1965



Engineering Experiment Station  
GEORGIA INSTITUTE OF TECHNOLOGY  
Atlanta, Georgia

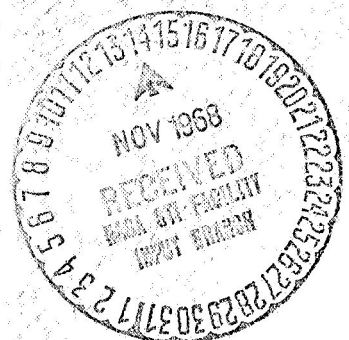


## TABLE OF CONTENTS

	Page
SUMMARY . . . . .	iv
NOMENCLATURE . . . . .	v
1. INTRODUCTION . . . . .	1
2. ANALYTICAL DETERMINATION OF THE PRESSURE DISTRIBUTION . . . . .	4
2.1. Free Oscillations . . . . .	5
2.2. Translational Oscillations . . . . .	8
2.3. Pitching and Yawing Oscillations . . . . .	11
2.4. Roll Oscillations . . . . .	14
3. INTRODUCTION OF DAMPING . . . . .	17
4. SPECIAL CONTAINERS . . . . .	19
4.1. Pressure Distribution in Multi-Cell Tank of Eight Cells .	19
4.2. Pressure Distribution in Multi-Cell Tank of Ten Cells . .	24
4.3. Pressure Distribution in Multi-Cell Tank of Twelve Cells.	29
5. ESTIMATE OF ERROR . . . . .	37
6. CONCLUSIONS . . . . .	42
7. REFERENCES . . . . .	44

# LIST OF FIGURES

	Page
1. Cross-Section of Multi-cell Container . . . . .	45
2. Container Geometry and Coordinate System . . . . .	46
3. Comparison of rectangular and circular container . . . . .	47
4. Pressure difference of rectangular and circular container at $\varphi = 0$ . . . . .	48
5. Pressure difference of rectangular and circular container at $\varphi = \pi/8$ . . . . .	49
6. Pressure difference of rectangular and circular container at $\varphi = \pi/4$ . . . . .	50
7. Fundamental Liquid frequency versus equivalent Reynolds number.	51

## SUMMARY

For propellant containers of large space boosters a multi-cell configuration has great structural and dynamic advantages. For this type of propellant containers the pressure distribution at the circular wall, the webs, and the tank bottom has been analytically derived for an arbitrary vertex angle of  $2\pi\alpha$ . Several excitation modes have been considered, such as free and forced propellant oscillations. The pressure response of the propellant to translational excitation in x- and y-direction, pitching and yawing excitations, as well as roll excitation about the longitudinal axis have been determined. The results have been applied to the multi-cell configuration of 8, 10 and 12 cells. The error involved in a slight geometry deviation has been estimated and found to be negligible for all practical purposes. The effect of amount of perforation and hole size of the perforation has also been stated.

# NOMENCLATURE

$a$	radius of container
$d$	baffle depth; diameter of perforation hole
$g$	longitudinal acceleration of vehicle, or gravity constant
$h$	liquid height
$i = \sqrt{-1}$	imaginary unit
$p$	pressure
$r, \varphi, z$	cylindrical polar coordinates
$t$	time
$w$	width of baffle
$x_o$	excitation amplitude for harmonic excitation in x-direction
$y_o$	excitation amplitude for harmonic excitation in y-direction
$J_{\frac{m}{2\alpha}}$	Bessel function of first kind and $(\frac{m}{2\alpha})^{\text{th}}$ order
$2\pi\alpha$	vertex angle of sector tank
$\beta$	effective baffle area
$\gamma_n$	liquid damping factor
$\epsilon_{mn}$	roots of first derivative of Bessel function $J_{m/2\alpha} - [J'_{m/2\alpha}(\epsilon_{mn}) = 0]$
$\Omega$	circular forcing frequency
$\omega_{mn}$	circular natural frequency of liquid
$\eta_{mn} = \frac{\Omega}{\omega_{mn}}$	frequency ratio of forcing to natural frequency
$\rho$	mass density of liquid
$\theta_o$	angular excitation amplitude in pitching excitation
$\chi_o$	angular excitation amplitude in yawing excitation
$\varphi_o$	angular excitation amplitude in roll excitation
$\zeta_w$	liquid surface amplitude at the container wall
$\Psi$	velocity potential of liquid in rectangular container
$\Phi$	velocity potential of liquid in circular cylinder

## 1. INTRODUCTION

As space vehicles have increased in size, their larger tank diameters have lowered the natural frequencies of the liquid propellants contained within, thus making the effects of propellant sloshing upon the stability of the vehicle more critical, especially at launch, where more than 90% of the total vehicle mass is usually in the form of liquid propellant and the sloshing masses exhibit considerable values for large container diameters. Employment of multi-cell configurations instead of the conventional circular cylindrical shell structures will reduce sloshing. The introduction of longitudinal radial wall into the container will reduce the sloshing masses and increase the natural frequencies slightly. Another possibility is the clustering of tanks with smaller diameters, which, however, has the disadvantage of a weight penalty.

In 1929 H. Oberth [1] recommended multi-cell propellant configurations for space vehicles. Recently J. F. Blumrich performed various studies for the application of multi-cell propellant containers [2, 3]. The cross section of such a typical multi-cell container is presented in Figure 1. The partial cylinders that form the periphery of the container may be of monocoque, stiffened, or honey comb construction. Stiffened webs extend radially from a center tube to the juncture of two outer tank sections and extend longitudinally between the cell end closure bulkheads. The webs can be perforated to allow pressure and propellant equalization between the various cells. The amount of perforation and its hole size, however, have to be chosen in such a fashion that the properties of the multi-cell construction, at least with respect to the propellant behavior, are preserved. This means that the sloshing masses and natural frequencies of the multi-cell are maintained. Holes too large would only result in the propellant behaving as in a conventional circular

cylindrical tank with some (from the standpoint of weight) costly additional damping of the propellant. Each radial web is attached to the outer partial cylinder juncture and to the upper and lower adjacent bulkheads by means of extruded Y sections. Along the periphery of the cross section, the partial cylinder walls are attached to the spherical transition sections and to the skirt by means of partial Y sections.

The multi-cell configurations have the following advantages over the conventional circular cylindrical shapes: (1) The radial webs, which are already present as part of the structure, enhance the stability of the space vehicle with respect to sloshing. (2) They prevent rotary sloshing. (3) Large multi-cell boosters can be designed so that weldments require only single pass welds, whereas circular cylindrical boosters of comparable volume and size require multiple pass welds. (4) Multi-cell construction offers flexibility in selection of tank diameters and bulkhead arrangements, thereby making it possible to use existing facilities for the purpose of manufacturing sections of a multi-cell container of a vehicle. (5) A weight saving occurs, as could be shown by comparison of large multi-cell and circular cylindrical space booster configurations. This indicates, in addition, a somewhat shorter vehicle for a multi-cell configuration, which probably could also mean a larger fundamental bending frequency, which is a desirable feature for the purpose of stability and control. (6) It is possible with a multi-cell configuration, to minimize fuel residuals, shorten skirt sections and suction lines, and obtain a shorter and lighter thrust structure. (7) Finally, the multi-cell concept can be adapted to lifting body shapes as needed for recoverable boosters.

In the following, emphasis is placed on the determination of dynamic fluid pressures for various multi-cell configurations. For a more lucid analytical

presentation a circular cylindrical sector container is treated. The pressure distribution in the container due to free and forced oscillations (translational, pitching, yawing, and roll-excitations) is determined for an arbitrary vertex angle  $2\pi\alpha$ . The results are then applied to the multi-cell configurations of 8, 10, and 12 cells. Since the propellant is treated as a frictionless liquid the magnification functions of the pressure distribution exhibit singularities at the resonances. In the vicinity of these, however, finite maximum values occur which influence the design of webs and container considerably. An exact solution of damped liquid vibrations is practically impossible, but a good approximation can be obtained by treating each vibration mode of the liquid as a one degree of freedom system and representing it as a spring-mass system. Since the mode shapes are not considerably changed by the present small damping of the liquids, an equivalent linear damping can be introduced easily in the resonance terms.

## 2. ANALYTICAL DETERMINATION OF THE PRESSURE DISTRIBUTION

The stability of liquid propelled space vehicles is adversely affected by the motion of the propellant in the tanks. In order to remedy this situation, subdivision of the propellant containers by longitudinal walls may be necessary for large space boosters. This increases the natural frequency of the propellant motion and decreases its sloshing masses considerably, thus avoiding strong dynamic coupling between the propellant and the structure and thereby making stability and control easier [4,5]. Because of the particular geometry of the multi-cell container, an investigation of the dynamic pressures for various excitations of the container is performed in order to predict the loads on the outer as well as on the cell walls of the container. By knowing the pressure distributions due to the motion of the propellant, a better structural optimization can be made for the container, thus saving structural weight for the space booster.

The pressure distribution in a circular cylindrical sector container is therefore derived for an arbitrary vertex angle  $2\pi\alpha$  for free and forced oscillations. Since, only translational, pitching, yawing, and roll excitations are of major importance, in the control and guidance maneuvers, the analysis was restricted to those motions. The multi-cell container is approximated by a circular cylindrical sector container arrangement for which several special cases, as the 1/8, 1/10, and 1/12 sector tank, are investigated. The results of the theory then will be applied to the total tank system for various orientations of the excitation. Special emphasis will be devoted to the 1/10-multi-cell tank arrangement, as this will be verified by experimental results at the George C. Marshall Space Flight Center, NASA, Huntsville, Alabama.

To determine the pressure distribution along the webs and walls of a circular cylindrical sector tank with a free fluid surface, potential theory [4] with linearized boundary conditions has been used\*. The main excitations that shall be considered here are translational harmonic excitation, pitching and yawing oscillations, as well as rolling excitations of various exciting frequencies. The flow field of the liquid with a free fluid surface in a cylindrical container of circular sector cross section, a vertex angle of  $2\pi\alpha$ , and a flat tank bottom (Fig. 2) has been obtained for a special case by Bauer by special limit considerations [4,5].

### 2.1. Free Oscillations.

The velocity potential for free liquid oscillation is given by

$$(2.1) \quad \Phi(r, \varphi, z, t) = \sum_{m=0}^{\infty} \sum_{n=0}^{\infty} \left[ A_{mn} \cos(\omega_{mn} t) + B_{mn} \sin(\omega_{mn} t) \right] \frac{\cosh\left[\epsilon_{mn} \left(\frac{z}{a} + \frac{h}{a}\right)\right]}{\cosh\left(\epsilon_{mn} \frac{h}{a}\right)} J_m\left(\epsilon_{mn} \frac{r}{a}\right) \cos\left(\frac{m}{2\alpha} \varphi\right)$$

where  $A_{mn}$  and  $B_{mn}$  are constants that have to be determined from the initial conditions. The expression  $\omega_{mn}$  is the natural circular frequency of the liquid and is

$$(2.2) \quad \omega_{mn}^2 = \frac{g}{a} \epsilon_{mn} \tanh\left(\epsilon_{mn} \frac{h}{a}\right) \quad \text{for } m, n = 0, 1, 2, 3, \dots$$

The values  $\epsilon_{mn}$  are the positive roots of  $\frac{J'_m}{2\alpha}(\epsilon_{mn}) = 0$ , and  $A_{mn}$  and  $B_{mn}$  are constants which are determined by the initial displacement and velocity of the free fluid surface. If the free fluid surface at the time  $t = 0$  has an initial

---

\*The fact that linearized theory can be used for these investigations and can give good results has been observed for the fluid forces of a quarter tank and  $45^\circ$  segmented container. [6,7]

displacement

$$\bar{z} = -\frac{1}{g} \left( \frac{\partial \Phi}{\partial t} \right)_{z=0} = f(r, \varphi)$$

and the initial velocity

$$\dot{\bar{z}} = g(r, \varphi)$$

and if  $f(r, \varphi)$  and  $g(r, \varphi)$  are expanded in Bessel-Fourier series of the form

$$f(r, \varphi) = \sum_{m=0}^{\infty} \sum_{n=0}^{\infty} f_{mn} J_{m/2\alpha} \left( \epsilon_{mn} \frac{r}{a} \right) \cos\left(\frac{m}{2\alpha} \varphi\right)$$

$$g(r, \varphi) = \sum_{m=0}^{\infty} \sum_{n=0}^{\infty} g_{mn} J_{m/2\alpha} \left( \epsilon_{mn} \frac{r}{a} \right) \cos\left(\frac{m}{2\alpha} \varphi\right)$$

the constants  $A_{mn}$  and  $B_{mn}$  can be determined in terms of the expansion constants  $f_{mn}$  and  $g_{mn}$ . It is

$$A_{mn} = \frac{g_{mn}}{\frac{\epsilon_{mn}}{a} \tanh \left( \epsilon_{mn} \frac{h}{a} \right)}$$

$$B_{mn} = -\frac{f_{mn} g}{\omega_{mn}}$$

The pressure distribution in the liquid at a depth  $(-z)$  is therefore ( $\rho$  as mass density of the liquid)

$$p = -\rho \frac{\partial \Phi}{\partial t} - \rho g z$$

where the last term represents the static pressure, while the first term is the dynamic (linearized) pressure. It is therefore:

$$(2.3) \quad p = \rho \sum_{m=0}^{\infty} \sum_{n=0}^{\infty} \omega_{mn} [A_{mn} \sin(\omega_{mn} t) - B_{mn} \cos(\omega_{mn} t)] \frac{\cosh[\epsilon_{mn}(\frac{z}{a} + \frac{h}{a})]}{\cosh(\epsilon_{mn} \frac{h}{a})} J_{m/2\alpha}$$

$$(\epsilon_{mn} \frac{r}{a}) \cos(\frac{m}{2\alpha} \varphi) - \rho g z$$

The pressure distribution for free oscillation on the cylindrical wall of the container is obtained from (2.3) for  $r = a$  and yields:

$$(2.4) \quad p_{wall} = \rho \sum_{m=0}^{\infty} \sum_{n=0}^{\infty} \omega_{mn} [A_{mn} \sin(\omega_{mn} t) - B_{mn} \cos(\omega_{mn} t)] \frac{\cosh[\epsilon_{mn}(\frac{z}{a} + \frac{h}{a})]}{\cosh(\epsilon_{mn} \frac{h}{a})} J_{m/2\alpha}$$

$$(\epsilon_{mn}) \cos(\frac{m}{2\alpha} \varphi) - \rho g z$$

At the webs the pressure distribution is at  $\varphi = 0$

$$(2.5) \quad p_{web \varphi=0} = \rho \sum_{m=0}^{\infty} \sum_{n=0}^{\infty} \omega_{mn} [A_{mn} \sin(\omega_{mn} t) - B_{mn} \cos(\omega_{mn} t)]$$

$$\frac{\cosh[\epsilon_{mn}(\frac{z}{a} + \frac{h}{a})]}{\cosh(\epsilon_{mn} \frac{h}{a})} J_{m/2\alpha} (\epsilon_{mn} \frac{r}{a}) - \rho g z$$

and at the web

$$(2.6) \quad p_{web} \varphi = 2\alpha\pi = \rho \sum_{m=0}^{\infty} \sum_{n=0}^{\infty} (-1)^n \omega_{mn} [A_{mn} \sin(\omega_{mn} t) - B_{mn} \cos(\omega_{mn} t)] \frac{\cosh[\epsilon_{mn}(\frac{z}{a} + \frac{h}{a})]}{\cosh(\epsilon_{mn} \frac{h}{a})} J_{\frac{m}{2\alpha}}(\epsilon_{mn} \frac{r}{a}) - \rho g z$$

The pressure distribution at the tank bottom yields with  $z = -h$  the expression

$$(2.7) \quad p_{bottom} = \rho \sum_{m=0}^{\infty} \sum_{n=0}^{\infty} \omega_{mn} [A_{mn} \sin(\omega_{mn} t) - B_{mn} \cos(\omega_{mn} t)] \frac{J_{m/2\alpha}(\epsilon_{mn} \frac{r}{a})}{\cosh(\epsilon_{mn} \frac{h}{a})} \cos(\frac{m}{2\alpha} \varphi) + \rho g h$$

From these results all special cases, such as 1/8, 1/10, and 1/12 sector tank, can be obtained and will be given later. (see section 4)

## 2.2. Translational Oscillations.

Excitation of the container along the x and y axis with an excitation frequency  $\Omega$  yields the velocity potential

$$(2.8) \quad \Phi(r, \varphi, z, t) = i\Omega e^{i\Omega t} \left\{ \begin{bmatrix} x_o r \cos \varphi \\ y_o r \sin \varphi \end{bmatrix} + \sum_{m=0}^{\infty} \sum_{n=0}^{\infty} \frac{\begin{bmatrix} a_m \bar{x}_o \\ c_m y_o \end{bmatrix} b_{mn} J_{m/2\alpha} \left( c_{mn} \frac{r}{a} \right) \eta_{mn}^2 \cosh \left[ \epsilon_{mn} \left( \frac{z}{a} + \frac{h}{a} \right) \right]}{(1 - \eta_{mn}^2) \cosh \left( \epsilon_{mn} \frac{h}{a} \right)} \cos \left( \frac{m}{2\alpha} \varphi \right) \right\}$$

where  $\eta_{mn} = \frac{\Omega}{\omega_{mn}}$  is the ratio of forcing frequency to the natural frequency.

The upper line in the large rectangular brackets belongs to the excitation  $x_o e^{i\Omega t}$  in x-direction, while the lower one belongs to the excitation  $y_o e^{i\Omega t}$  in y-direction. It is

$$(2.9) \quad a_o = \frac{\sin 2\pi\alpha}{2\pi\alpha} \quad c_o = \frac{1 - \cos 2\pi\alpha}{2\pi\alpha}$$

$$a_m = \frac{4\alpha (-1)^{m+1} \sin 2\pi\alpha}{\pi[m^2 - 4\alpha^2]} \quad c_m = \frac{4\alpha [(-1)^m \cos 2\pi\alpha - 1]}{\pi[m^2 - 4\alpha^2]}$$

and

$$(2.10) \quad b_{mn} = \frac{2a \frac{\Gamma(\frac{m}{4\alpha} + \frac{3}{2})}{\Gamma(\frac{m}{4\alpha} - \frac{1}{2})} \sum_{\mu=0}^{\infty} \frac{(\frac{m}{2\alpha} + 2\mu + 1) \Gamma(\frac{m}{4\alpha} + \mu - \frac{1}{2})}{\Gamma(\frac{m}{4\alpha} + \mu + \frac{5}{2})} J_{m/2\alpha + 2\mu + 1}(\epsilon_{mn})}{\epsilon_{mn} \left(1 - \frac{m^2}{4\alpha^2 \epsilon_{mn}^2}\right) J_{m/2\alpha}^2(\epsilon_{mn})}$$

The pressure distribution then is

$$(2.11) \quad p = \rho \Omega^2 e^{i\Omega t} \left\{ \begin{bmatrix} x_o r \cos \varphi \\ y_o r \sin \varphi \end{bmatrix} + \sum_{m=0}^{\infty} \sum_{n=0}^{\infty} \frac{\begin{bmatrix} a_m x_o \\ c_m y_o \end{bmatrix} b_{mn} J_{\frac{m}{2\alpha}} \left( \epsilon_{mn} \frac{r}{a} \right) \eta_{mn}^2 \cosh \left[ \epsilon_{mn} \left( \frac{z}{a} + \frac{h}{a} \right) \right] \cos \left( \frac{m}{2\alpha} \varphi \right)}{(1 - \eta_{mn}^2) \cosh \left( \epsilon_{mn} \frac{h}{a} \right)} \right\} - \rho g z$$

At the cylindrical wall of the container the pressure distribution is given by

$$(2.12) \quad p_{\text{wall}} = \rho \Omega^2 e^{i\Omega t} \left\{ \begin{bmatrix} x_o a \cos \varphi \\ y_o a \sin \varphi \end{bmatrix} + \sum_{m=0}^{\infty} \sum_{n=0}^{\infty} \frac{\begin{bmatrix} a_m x_o \\ c_m y_o \end{bmatrix} b_{mn} J_{\frac{m}{2\alpha}} \left( \epsilon_{mn} \right) \eta_{mn}^2 \cosh \left[ \epsilon_{mn} \left( \frac{z}{a} + \frac{h}{a} \right) \right] \cos \left( \frac{m}{2\alpha} \varphi \right)}{(1 - \eta_{mn}^2) \cosh \left( \epsilon_{mn} \frac{h}{a} \right)} \right\} - \rho g z$$

At the webs the pressure distribution yields

$$(2.13) \quad p_{\text{web } \varphi = 0} = \rho \Omega^2 e^{i\Omega t} \left\{ \begin{bmatrix} x_o r \\ 0 \end{bmatrix} + \sum_{m=0}^{\infty} \sum_{n=0}^{\infty} \frac{\begin{bmatrix} a_m x_o \\ c_m y_o \end{bmatrix} b_{mn} J_{\frac{m}{2\alpha}} \left( \epsilon_{mn} \frac{r}{a} \right) \eta_{mn}^2 \cosh \left[ \epsilon_{mn} \left( \frac{z}{a} + \frac{h}{a} \right) \right]}{(1 - \eta_{mn}^2) \cosh \left( \epsilon_{mn} \frac{h}{a} \right)} \right\} - \rho g z$$

and

$$p_{web} \varphi = 2\pi\alpha = \rho\Omega^2 e^{i\Omega t} \left\{ \begin{bmatrix} x_o r \cos 2\pi\alpha \\ y_o r \sin 2\pi\alpha \end{bmatrix} \right.$$

(2.14)

$$+ \sum_{m=0}^{\infty} \sum_{n=0}^{\infty} \frac{\begin{bmatrix} a_m x_o \\ c_m y_o \end{bmatrix} b_{mn} (-1)^m J_{\frac{m}{2\alpha}} \left( \epsilon_{mn} \frac{r}{a} \right) \eta_{mn}^2 \cosh \left[ \epsilon_{mn} \left( \frac{z}{a} + \frac{h}{a} \right) \right]}{(1 - \eta_{mn}^2) \cosh \left( \epsilon_{mn} \frac{h}{a} \right)} \left. \right\} - \rho g z$$

The pressure distribution at the tank bottom for translational excitation is given by the expression

$$(2.15) \quad p_{bottom} = \rho\Omega^2 e^{i\Omega t} \left\{ \begin{bmatrix} x_o r \cos \varphi \\ y_o r \sin \varphi \end{bmatrix} \right. \\ \left. + \sum_{m=0}^{\infty} \sum_{n=0}^{\infty} \frac{\begin{bmatrix} a_m x_o \\ c_m y_o \end{bmatrix} b_{mn} J_{\frac{m}{2\alpha}} \left( \epsilon_{mn} \frac{r}{a} \right) \eta_{mn}^2 \cos \left( \frac{m}{2\alpha} \varphi \right)}{(1 - \eta_{mn}^2) \cosh \left( \epsilon_{mn} \frac{h}{a} \right)} \right\} + \rho g z$$

### 2.3. Pitching and Yawing Oscillations.

If the container is excited about the  $\xi$  or  $\eta$  axis (see Figure 2),  $\chi_o e^{i\Omega t}$  or  $\theta_o e^{i\Omega t}$  respectively is the potential of the liquid yields for pitching  $\theta$ , upper line) and yawing ( $\chi$ , lower line).

$$(2.16) \quad \Phi(r, \varphi, z, t) = -i\Omega e^{i\Omega t} \left\{ \begin{bmatrix} \theta_o r z \cos \varphi \\ \chi_o r z \sin \varphi \end{bmatrix} - \begin{bmatrix} \theta_o \\ \chi_o \end{bmatrix} \right.$$

$$\sum_{m=0}^{\infty} \sum_{n=0}^{\infty} [C_{mn} \cosh(\epsilon_{mn} \frac{z}{a}) + D_{mn} \sinh(\epsilon_{mn} \frac{z}{a})] J_{\frac{m}{2\alpha}} \left( \epsilon_{mn} \frac{r}{a} \right) \cdot \\ \cdot \cos \left( \frac{m}{2\alpha} \varphi \right)$$

where

$$C_{mn} = \frac{ab_{mn} \eta_{mn}^2}{\epsilon_{mn}(1-\eta_{mn}^2) \cosh(\epsilon_{mn} \frac{h}{a})}$$

$$\left[ 2 \sinh \left( \frac{\epsilon_{mn}}{2} \frac{h}{a} \right) - \left( \frac{\epsilon_{mn}}{2} \frac{h}{a} + \frac{g\epsilon_{mn}}{a\Omega^2} \right) \cosh \left( \frac{\epsilon_{mn}}{2} \frac{h}{a} \right) \right] \begin{bmatrix} a_m \\ c_m \end{bmatrix}$$

(2.17)

$$D_{mn} = \frac{ab_{mn} \eta_{mn}^2}{\epsilon_{mn}(1 - \eta_{mn}^2) \cosh(\epsilon_{mn} \frac{h}{a})}$$

$$\left[ \left( \frac{g\epsilon_{mn}}{a\Omega^2} - \frac{\epsilon_{mn} h}{2a} \right) \sinh \left( \frac{\epsilon_{mn}}{2} \frac{h}{a} \right) - 2 \sinh \left( \frac{\epsilon_{mn}}{2} \frac{h}{a} \right) \right] \begin{bmatrix} a_m \\ c_m \end{bmatrix}$$

The pressure distribution is then

$$(2.18) \quad p = \rho\Omega^2 e^{i\Omega t} \left\{ \begin{bmatrix} \theta_o r z \cos \varphi \\ x_o r z \sin \varphi \end{bmatrix} - \begin{bmatrix} \theta_o \\ x_o \end{bmatrix} \right.$$

$$\left. \sum_{m=0}^{\infty} \sum_{n=0}^{\infty} \left[ C_{mn} \cosh(\epsilon_{mn} \frac{z}{a}) + D_{mn} \sinh(\epsilon_{mn} \frac{z}{a}) \right] J_{\frac{m}{2\alpha}}(\epsilon_{mn} \frac{r}{a}) \cos \left( \frac{m}{2\alpha} \varphi \right) \right\}$$

$$- \rho g(z - \frac{h}{2})$$

At the circular wall  $r = a$  the pressure distribution is

$$(2.19) \quad p_{wall} = \rho\Omega^2 e^{i\Omega t} \left\{ \begin{bmatrix} \theta_o a z \cos \varphi \\ x_o a z \sin \varphi \end{bmatrix} - \begin{bmatrix} \theta_o \\ x_o \end{bmatrix} \right.$$

$$\left. \sum_{m=0}^{\infty} \sum_{n=0}^{\infty} \left[ C_{mn} \cosh(\epsilon_{mn} \frac{z}{a}) + D_{mn} \sinh(\epsilon_{mn} \frac{z}{a}) \right] J_{\frac{m}{2\alpha}}(\epsilon_{mn}) \cos \left( \frac{m}{2\alpha} \varphi \right) \right\}$$

$$- \rho g(z - \frac{h}{2})$$

At the webs it is

$$(2.20) \quad p_{web \quad \varphi=0} = - \rho \Omega^2 e^{i\Omega t} \left\{ \begin{bmatrix} \theta_o r z \\ 0 \end{bmatrix} - \begin{bmatrix} \theta_o \\ \chi_o \end{bmatrix} \right. \\
\left. \sum_{m=0}^{\infty} \sum_{n=0}^{\infty} [C_{mn} \cosh(\epsilon_{mn} \frac{z}{a}) + D_{mn} \sinh(\epsilon_{mn} \frac{z}{a})] J_{\frac{m}{2\alpha}}(\epsilon_{mn} \frac{r}{a}) \right\} \\
- \rho g(z - \frac{h}{2})$$

and at  $\varphi = 2\pi\alpha$  the pressure distribution yields

$$(2.21) \quad p_{web \quad \varphi=2\pi\alpha} = - \rho \Omega^2 e^{i\Omega t} \left\{ \begin{bmatrix} \theta_o r z \cos 2\pi\alpha \\ \chi_o r z \sin 2\pi\alpha \end{bmatrix} - \begin{bmatrix} \theta_o \\ \chi_o \end{bmatrix} \right. \\
\left. \sum_{m=0}^{\infty} \sum_{n=0}^{\infty} [C_{mn} \cosh(\epsilon_{mn} \frac{z}{a}) + D_{mn} \sinh(\epsilon_{mn} \frac{z}{a})] (-1)^m J_{\frac{m}{2\alpha}}(\epsilon_{mn} \frac{r}{a}) \right\} \\
- \rho g(z - \frac{h}{2})$$

The pressure distribution at the container bottom is

$$(2.22) \quad p_{bottom} = - \rho \Omega^2 e^{i\Omega t} \left\{ \begin{bmatrix} -\theta_o r \frac{h}{2} \cos \varphi \\ -\chi_o r \frac{h}{2} \sin \varphi \end{bmatrix} - \begin{bmatrix} \theta_o \\ \chi_o \end{bmatrix} \right. \\
\left. \sum_{m=0}^{\infty} \sum_{n=0}^{\infty} [C_{mn} \cosh(\frac{\epsilon_{mn}}{2} \frac{h}{a}) - D_{mn} \sinh(\frac{\epsilon_{mn}}{2} \frac{h}{a})] J_{\frac{m}{2\alpha}}(\epsilon_{mn} \frac{r}{a}) \cos(\frac{m}{2\alpha} \varphi) \right\} \\
+ \rho gh$$

It should be noted in this section that the coordinate system has its origin in the vertex axis in the middle between the tank bottom and the quiescent fluid surface. All special cases and orientations of a multi-cell tank system can be obtained from these results by superposition of the above results.

#### 2.4. Roll Oscillations.

For roll excitation  $\varphi = \varphi_0 e^{i\Omega t}$  about the z axis (here the origin is again located in the quiescent fluid surface) the velocity potential yields:

$$(2.25) \quad \Phi(r, \varphi, z, t) = i\Omega a^2 \varphi_0 e^{i\Omega t} \left[ \left( \frac{r}{a} \right)^2 (\varphi - \pi\alpha) + \sum_{m=1}^{\infty} \frac{16\alpha \cos \left( \frac{2m-1}{2\alpha} \varphi \right)}{\pi^2 [(2m-1)^2 - 16\alpha^2] (2m-1)} \right]$$

$$\begin{aligned} & \left[ \left( \frac{r}{a} \right)^{\frac{2m-1}{2\alpha}} - \frac{4\alpha}{(2m-1)} \left( \frac{r}{a} \right)^2 \right] + \sum_{m=0}^{\infty} \sum_{n=0}^{\infty} \\ & \frac{8\alpha \left[ \frac{4\alpha}{2m-1} f_{2m-1,n} - e_{2m-1,n} \right] J_{\frac{2m-1}{2\alpha}} \left( \epsilon_{2m-1,n} \frac{r}{a} \right) \eta_{2m-1,n}^2}{\pi [(2m-1)^2 - 16\alpha^2] (1 - \eta_{2m-1,n}^2) \cosh \left( \epsilon_{2m-1,n} \frac{h}{a} \right)} \\ & \cosh \left[ \epsilon_{2m-1,n} \left( \frac{z}{a} + \frac{h}{a} \right) \right] \cos \left( \frac{2m-1}{2\alpha} \varphi \right) \end{aligned}$$

where

$$\begin{aligned} (2.26) \quad f_{2m-1,n} &= \frac{2 \left( \frac{2m-1}{2\alpha} \right)}{[\epsilon_{2m-1,n}^2 - \left( \frac{2m-1}{2\alpha} \right)^2] J_{\frac{2m-1}{2\alpha}} (\epsilon_{2m-1,n})} \\ e_{2m-1,n} &= \frac{2\epsilon_{2m-1,n} \left( \frac{2m-1}{4\alpha} \right) \left( \frac{2m-1}{4\alpha} - 1 \right) \left( \frac{2m-1}{4\alpha} + 1 \right)}{[\epsilon_{2m-1,n}^2 - \left( \frac{2m-1}{2\alpha} \right)^2] J_{\frac{2m-1}{2\alpha}}^2 (\epsilon_{2m-1,n})} \sum_{\mu=0}^{\infty} \\ & \frac{\left( \frac{2m-1}{2\alpha} + 2\mu + 1 \right) J_{\frac{2m-1}{2\alpha} + 2\mu + 1} (\epsilon_{2m-1,n})}{\left( \frac{2m-1}{4\alpha} + \mu - 1 \right) \left( \frac{2m-1}{4\alpha} + \mu \right) \left( \frac{2m-1}{4\alpha} + \mu + 1 \right) \left( \frac{2m-1}{4\alpha} + \mu + 2 \right)} \end{aligned}$$

The pressure distribution in the container is then

$$\begin{aligned}
(2.27) \quad p = \rho \Omega_a^2 \varphi_0 e^{i\Omega t} & \left\{ \left( \frac{r}{a} \right)^2 (\varphi - \alpha\pi) + \sum_{n=1}^{\infty} \frac{16\alpha \cos \left( \frac{2m-1}{2\alpha} \varphi \right)}{\pi^2 (2m-1) [(2m-1)^2 - 16\alpha^2]} \right. \\
& \left[ \left( \frac{r}{a} \right)^{\frac{2m-1}{2\alpha}} - \frac{4\alpha}{(2m-1)} \left( \frac{r}{a} \right)^2 \right] + \sum_{m=1}^{\infty} \sum_{n=0}^{\infty} \\
& \frac{8\alpha \left[ \frac{4\alpha}{2m-1} f_{2m-1,n} - e_{2m-1,n} \right] J_{\frac{2m-1}{2\alpha}} (\epsilon_{2m-1,n} \frac{r}{a}) \eta_{2m-1,n}^2 \cosh[\epsilon_{2m-1,n} (\frac{z}{a} + \frac{h}{a})]}{(1 - \eta_{2m-1,n}^2) \cosh(\epsilon_{2m-1,n} \frac{h}{a}) \pi [(2m-1)^2 - 16\alpha^2]} \\
& \left. \cos \left( \frac{2m-1}{2\alpha} \varphi \right) \right\} - \rho g z
\end{aligned}$$

and the pressure distribution at the circular wall is

$$\begin{aligned}
(2.28) \quad p_{wall} = \rho \Omega_a^2 \varphi_0 e^{i\Omega t} & \left[ (\varphi - \pi\alpha) + \frac{16\alpha}{\pi^2} \sum_{m=1}^{\infty} \frac{\cos \left( \frac{2m-1}{2\alpha} \varphi \right)}{(2m-1)^2 [(2m-1) + 4\alpha]} + \frac{8\alpha}{\pi} \sum_{m=1}^{\infty} \sum_{n=0}^{\infty} \right. \\
& \left. \frac{(\frac{4\alpha}{2m-1} f_{2m-1,n} - e_{2m-1,n}) J_{\frac{2m-1}{2\alpha}} (\epsilon_{2m-1,n}) \eta_{2m-1,n}^2 \cosh[\epsilon_{2m-1,n} (\frac{z}{a} + \frac{h}{a})] \cos(\frac{2m-1}{2\alpha} \varphi)}{[(2m-1)^2 - 16\alpha^2] (1 - \eta_{mn}^2) \cosh(\epsilon_{2m-1,n} \frac{h}{a})} \right] \\
& - \rho g z
\end{aligned}$$

At the webs the pressure distribution is given by

$$(2.29) \quad p_{web \varphi=0} = \rho \Omega^2 a^2 \varphi_0 e^{i\Omega t} \left[ -\left(\frac{r}{a}\right)^2 \alpha \pi + \frac{16\alpha}{\pi^2} \sum_{m=1}^{\infty} \frac{\left[\left(\frac{r}{a}\right)^{\frac{2m-1}{2\alpha}} - \frac{4\alpha}{(2m-1)} \left(\frac{r}{a}\right)^2\right]}{(2m-1) [(2m-1)^2 - 16\alpha^2]} + \frac{8\alpha}{\pi} \sum_{m=1}^{\infty} \sum_{n=0}^{\infty} \right.$$

$$\left. \frac{\left[\frac{4\alpha}{(2m-1)} f_{2m-1,n} - e_{2m-1,n}\right] J_{\frac{2m-1}{2\alpha}} \left(\epsilon_{2m-1,n} \frac{r}{a}\right) \eta_{2m-1,n}^2 \cosh\left[\epsilon_{2m-1,n} \left(\frac{z}{a} + \frac{h}{a}\right)\right]}{[(2m-1)^2 - 16\alpha^2] (1 - \eta_{2m-1,n}^2) \cosh\left(\epsilon_{2m-1,n} \frac{h}{a}\right)} \right] - \rho g z$$

and

$$(2.30) \quad p_{web \varphi=2\pi\alpha} = \rho \Omega^2 a^2 \varphi_0 e^{i\Omega t} \left[ \left(\frac{r}{a}\right)^2 \pi \alpha - \frac{16\alpha}{\pi^2} \sum_{m=1}^{\infty} \frac{\left[\left(\frac{r}{a}\right)^{\frac{2m-1}{2\alpha}} - \frac{4\alpha}{(2m-1)} \left(\frac{r}{a}\right)^2\right]}{(2m-1) [(2m-1)^2 - 16\alpha^2]} - \frac{8\alpha}{\pi} \sum_{m=1}^{\infty} \sum_{n=0}^{\infty} \right.$$

$$\left. \frac{\left[\frac{4\alpha}{2m-1} f_{2m-1,n} - e_{2m-1,n}\right] J_{\frac{2m-1}{2\alpha}} \left(\epsilon_{2m-1,n} \frac{r}{a}\right) \eta_{2m-1,n}^2 \cosh\left[\epsilon_{2m-1,n} \left(\frac{z}{a} + \frac{h}{a}\right)\right]}{[(2m-1)^2 - 16\alpha^2] (1 - \eta_{2m-1,n}^2) \cosh\left(\epsilon_{2m-1,n} \frac{h}{a}\right)} \right] - \rho g z$$

The pressure distribution at the container bottom yields

$$(2.31) \quad p_{bottom} = \rho \Omega^2 a^2 \varphi_0 e^{i\Omega t} \left[ \left(\frac{r}{a}\right)^2 (\varphi - \pi \alpha) + \sum_{m=1}^{\infty} \frac{16\alpha \cos\left(\frac{2m-1}{2\alpha} \varphi\right)}{R^2 (2m-1) [(2m-1)^2 - 16\alpha^2]} \right.$$

$$\left. \left[ \left(\frac{r}{a}\right)^{\frac{2m-1}{2\alpha}} - \frac{4\alpha}{2m-1} \left(\frac{r}{a}\right)^2 \right] + \sum_{m=1}^{\infty} \sum_{n=0}^{\infty} \frac{8\alpha}{\pi} \right.$$

$$\left. \frac{\left[\frac{4\alpha}{2m-1} f_{2m-1,n} - e_{2m-1,n}\right] J_{\frac{2m-1}{2\alpha}} \left(\epsilon_{2m-1,n} \frac{r}{a}\right) \eta_{2m-1,n}^2 \cos\left(\frac{2m-1}{2\alpha} \varphi\right)}{(1 - \eta_{2m-1,n}^2) \cosh\left(\epsilon_{2m-1,n} \frac{h}{a}\right) [(2m-1)^2 - 16\alpha^2]} \right] + \rho g z$$

From these results all special cases, such as 1/8, 1/10, and 1/12 multi-cell container, can be obtained and will be presented in explicit form later (see section 4).

### 3. INTRODUCTION OF DAMPING

In a frictionless liquid (Section 2) the magnification function of the pressure distribution exhibits singularities at the resonances. That is, at a forcing frequency  $\Omega = \omega_{mn}$  the magnitude of the pressure tends toward infinity. All previous results are therefore not applicable in the immediate vicinity of these Eigenfrequencies of the system. In fact, finite values occur in the resonances and are due to the damping of the liquid, which has been neglected in the potential theory solution of the problem. An exact solution of damped liquid oscillations is practically impossible and another approach must be chosen to account for damping.

Considering each vibrational mode of the fluid as a degree of freedom and representing it as a spring-mass system, damping can be introduced in the analytical results of the potential flow theory by rewriting the resonance terms  $(1 - \eta_n^2)$  as a complex expression  $(1 - \eta_n^2 + 2i \gamma_n \eta_n)$ , where  $i$  is the imaginary unit and  $\gamma_n$  is the damping factor associated with this particular vibrational mode. With this approach linear velocity proportional damping has been introduced. The values  $\gamma_n$  have to be obtained by experiments and are in a smooth walled container usually of a magnitude in the order of  $0.001 < \gamma < 0.02$ . With baffles in the container the damping can be obtained by a semi-empirical formula by Miles, which has been improved by Bauer [6]. It is

$$(3.1) \quad \gamma = C_e^{-4.6} \frac{d}{a} \bar{\beta}^{3/2} \sqrt{\zeta_w/a}$$

where  $d$  is the depth of the baffle below the quiescent free fluid surface,  $\zeta_w$  is the maximum free fluid surface displacement at the container wall, and  $\bar{\beta}$  is the effective baffle area ratio blocking the cross sectional area. The constant  $C$  is obtained from experimental drag measurements of flat plates in an oscil-

lating fluid and has approximately the value 2.8 in a circular cylinder. In a completely submerged ring baffle the baffle area is

$$\bar{\beta} = \frac{\alpha}{\pi a^2} [\pi a^2 - \pi(a-w)^2] = \frac{w}{a} [2 - \frac{w}{a}]$$

where  $w$  is the width of the ring baffle.

In the expressions (2.11) to (2.15) if one introduces now the value  $(1 - \eta_{mn}^2 + 2i \gamma_{mn} \eta_{mn})$  instead of  $(1 - \eta_{mn}^2)$  in the denominator of the double series, one obtains the pressure distribution for damped fluid oscillations. The same is true for the expressions (2.17) in the case of pitching and yawing excitations, and in (2.28) to (2.31) for the case of roll excitation.

From the measured response we will be able to obtain an approximate value for the damping factors  $\gamma_{mn}$ .

#### 4. SPECIAL CONTAINERS

In the equations of section 2, we now introduce the values  $\pi/4$ ,  $\pi/5$  and  $\pi/6$  for the vertex angle. This yields the pressure distribution for the multi-cell container of 8, 10, 12 cells.

##### 4.1. Pressure Distributions in Multi-Cell Tank of Eight Cells.

For a container of vertex angle  $\pi/4$  the value  $\alpha = 1/8$  and the pressure distributions for free oscillations are:

$$(4.1) \quad p_{\text{WALL}} = \rho \sum_{m=0}^{\infty} \sum_{n=0}^{\infty} \omega_{mn} [A_{mn} \sin(\omega_{mn} t) - B_{mn} \cos(\omega_{mn} t)] \frac{\cosh[\epsilon_{mn}(\frac{z+h}{a})]}{\cosh[\epsilon_{mn} \frac{h}{a}]} J_{4m}(\epsilon_{mn}) \cos 4m\varphi - \rho g z$$

where the  $\epsilon_{mn}$ 's are the zeros of  $J'_{4m}(\epsilon_{mn}) = 0$  and are represented in Table 1.

At the webs the pressure distributions are

$$(4.2) \quad p_{\text{WEB } \varphi=0} = \rho \sum_{m=0}^{\infty} \sum_{n=0}^{\infty} \omega_{mn} [A_{mn} \sin(\omega_{mn} t) - B_{mn} \cos(\omega_{mn} t)] \frac{\cosh[\epsilon_{mn}(\frac{z+h}{a})]}{\cosh(\epsilon_{mn} \frac{h}{a})} J_{4m}(\epsilon_{mn} \frac{r}{a}) - \rho g z$$

$$(4.3) \quad p_{\text{WEB } \varphi=\pi/4} = \rho \sum_{m=0}^{\infty} \sum_{n=0}^{\infty} (-1)^m \omega_{mn} [A_{mn} \sin(\omega_{mn} t) - B_{mn} \cos(\omega_{mn} t)] \frac{\cosh[\epsilon_{mn}(\frac{z+h}{a})]}{\cosh(\epsilon_{mn} \frac{h}{a})} J_{4m}(\epsilon_{mn} \frac{r}{a}) - \rho g z$$

The pressure distribution at the container bottom is

$$(4.4) \quad p_{\text{bottom}} = \rho \sum_{m=0}^{\infty} \sum_{n=0}^{\infty} \omega_{mn} [A_{mn} \sin(\omega_{mn} t) - B_{mn} \cos(\omega_{mn} t)] \frac{J_{4m}(\epsilon_{mn} \frac{r}{a})}{\cosh(\epsilon_{mn} \frac{h}{a})} \cos 4m\varphi + \rho gh$$

For translational excitation with

$$(4.5) \quad a_0 = \frac{2\sqrt{2}}{\pi}, \quad a_m = \frac{4\sqrt{2}(-1)^{m+1}}{\pi(16m^2 - 1)}, \quad c_0 = \frac{2[2-\sqrt{2}]}{\pi}, \quad c_m = \frac{4[(-1)^m\sqrt{2}-2]}{\pi(16m^2-1)}.$$

$$(4.6) \quad b_{mn} = \frac{4a\epsilon_{mn}(16m^2 - 1)}{(\epsilon_{mn}^2 - 16m^2) J_{4m}^2(\epsilon_{mn})} \sum_{\mu=0}^{\infty} \frac{J_{4m+2\mu+1}(\epsilon_{mn})}{(4m+2\mu-1)(4m+2\mu+3)}$$

the pressure distribution at the cylindrical wall of the container is

$$(4.7) \quad p_{\text{WALL}} = \rho \Omega^2 e^{i\Omega t} \left[ \begin{array}{l} x_0 a \cos \varphi \\ y_0 a \sin \varphi \end{array} \right] + \sum_{m=0}^{\infty} \sum_{n=0}^{\infty} \frac{\begin{bmatrix} x_0 a_m \\ y_0 c_m \end{bmatrix} b_{mn} J_{4m}(\epsilon_{mn}) \eta_{mn}^2 \cosh \left[ \epsilon_{mn} \left( \frac{z+h}{a} \right) \right] \cos 4m\varphi}{(1 - \eta_{mn}^2) \cosh(\epsilon_{mn} \frac{h}{a})} \right] - \rho gz$$

At the webs the pressure distribution is

$$(4.8) \quad p_{\text{WEB } \varphi=0} = \rho \Omega^2 e^{i\Omega t} \left[ \begin{bmatrix} x_o r \\ y_o c_m \end{bmatrix} + \sum_{m=0}^{\infty} \sum_{n=0}^{\infty} \frac{\begin{bmatrix} x_o a_m \\ y_o c_m \end{bmatrix} b_{mn} J_{4m} \left( \epsilon_{mn} \frac{r}{a} \right) \eta_{mn}^2 \cosh \left[ \epsilon_{mn} \left( \frac{z+h}{a} \right) \right]}{(1 - \eta_{mn}^2) \cosh \left( \epsilon_{mn} \frac{h}{a} \right)} \right] - \rho g z$$

$$(4.9) \quad p_{\text{WEB } \varphi=\pi/4} = \rho \Omega^2 e^{i\Omega t} \left[ \begin{bmatrix} \frac{x_o r}{2} \sqrt{2} \\ \frac{y_o r}{2} \sqrt{2} \end{bmatrix} + \sum_{m=0}^{\infty} \sum_{n=0}^{\infty} \frac{(-1)^m \begin{bmatrix} x_o a_m \\ y_o c_m \end{bmatrix} b_{mn} J_{4m} \left( \epsilon_{mn} \frac{r}{a} \right) \eta_{mn}^2 \cosh \left[ \epsilon_{mn} \left( \frac{z+h}{a} \right) \right]}{(1 - \eta_{mn}^2) \cosh \left( \epsilon_{mn} \frac{h}{a} \right)} \right] - \rho g z$$

At the container bottom the pressure distribution yields

$$(4.10) \quad p_{\text{bottom}} = \rho \Omega^2 e^{i\Omega t} \left[ \begin{bmatrix} x_o r \cos \varphi \\ y_o r \sin \varphi \end{bmatrix} + \sum_{m=0}^{\infty} \sum_{n=0}^{\infty} \frac{\begin{bmatrix} a_m x_o \\ c_m y_o \end{bmatrix} b_{mn} J_{4m} \left( \epsilon_{mn} \frac{r}{a} \right) \eta_{mn}^2 \cos 4m\varphi}{(1 - \eta_{mn}^2) \cosh \left( \epsilon_{mn} \frac{h}{a} \right)} \right] + \rho g h$$

For pitching and yawing excitation the pressure distribution at the cylindrical container wall is

$$(4.11) \quad p_{\text{WALL}} = -\rho\Omega^2 e^{i\Omega t} \left[ \begin{bmatrix} \theta_o a z \cos \varphi \\ \chi_o a z \sin \varphi \end{bmatrix} - \begin{bmatrix} \theta_o \\ \chi_o \end{bmatrix} \sum_{m=0}^{\infty} \sum_{n=0}^{\infty} [C_{mn} (\epsilon_{mn} \frac{z}{a}) + D_{mn} \sinh (\epsilon_{mn} \frac{z}{a})] J_{4m} (\epsilon_{mn}) \cos 4m\varphi \right] - \rho g(z - \frac{h}{2})$$

where the values  $C_{mn}$  and  $D_{mn}$  are given by the equations (2.17). For the appearing  $b_{mn}$  the expression (4.6) has to be introduced. The pressure distribution at the web,  $\varphi = 0$  and  $\varphi = \pi/4$ , is given by

$$(4.12) \quad p_{\text{WEB } \varphi=0} = -\rho\Omega^2 e^{i\Omega t} \left[ \begin{bmatrix} \theta_o r z \\ 0 \end{bmatrix} - \begin{bmatrix} \theta_o \\ \chi_o \end{bmatrix} \sum_{m=0}^{\infty} \sum_{n=0}^{\infty} [C_{mn} \cosh (\epsilon_{mn} \frac{z}{a}) + D_{mn} \sinh (\epsilon_{mn} \frac{z}{a})] J_{4m} (\epsilon_{mn} \frac{r}{a}) \right] - \rho g(z - \frac{h}{2})$$

$$(4.13) \quad p_{\text{WEB } \varphi=\pi/4} = -\rho\Omega^2 e^{i\Omega t} \left[ \begin{bmatrix} \theta_o r z \\ \frac{\chi_o r z}{\sqrt{2}} \end{bmatrix} - \begin{bmatrix} \theta_o \\ \chi_o \end{bmatrix} \sum_{m=0}^{\infty} \sum_{n=0}^{\infty} [C_{mn} \cosh (\epsilon_{mn} \frac{z}{a}) + D_{mn} \sinh (\epsilon_{mn} \frac{z}{a})] (-1)^m J_{4m} (\epsilon_{mn} \frac{r}{a}) \right] - \rho g(z - \frac{h}{2})$$

At the container bottom it is

$$(4.14) \quad p_{\text{bottom}} = -\rho\Omega^2 e^{i\Omega t} \left[ \begin{bmatrix} -\theta_o r \frac{h}{2} \cos \varphi \\ -\chi_o r \frac{h}{2} \sin \varphi \end{bmatrix} - \begin{bmatrix} \theta_o \\ \chi_o \end{bmatrix} \sum_{m=0}^{\infty} \sum_{n=0}^{\infty} [C_{mn} \cosh (\frac{\epsilon_{mn}}{a} \frac{h}{a}) + D_{mn} \sinh (\frac{\epsilon_{mn}}{2} \frac{h}{2})] J_{4m} (\epsilon_{mn} \frac{r}{a}) \cos 4m\varphi \right] + \rho gh$$

For roll excitation the pressure distribution at the cylindrical wall is

$$(4.15) \quad p_{\text{WALL}} = \rho \Omega^2 a^2 \varphi_0 e^{i\Omega t} \left[ (\varphi - \pi/8) + \frac{2}{\pi^2} \sum_{m=1}^{\infty} \frac{\cos (8m - 4) \varphi}{(2m-1)^2 [(2m-1)+1/2]} \right. \\ \left. + \frac{1}{\pi} \sum_{m=1}^{\infty} \sum_{n=0}^{\infty} \frac{(\frac{1}{4m-2} f_{2m-1,n} - e_{2m-1,n}) J_{8m-4}(\epsilon_{2m-1,n}) \eta_{2m-1,n}^2 \cosh[\epsilon_{2m-1,n} (\frac{z}{a} + \frac{h}{a})]}{[(2m-1)^2 - 1/4] (1 - \eta_{2m-1,n}^2) \cosh(\epsilon_{2m-1,n} \frac{h}{a})} \right. \\ \left. \cdot \cos (8m-4) \right] - \rho g z$$

The values  $f_{2m-1,n}$  and  $e_{2m-1,n}$  are given by

$$f_{2m-1,n} = \frac{8(2m-1)}{(\epsilon_{2m-1,n}^2 - 16(2m-1)^2) J_{8m-4}(\epsilon_{2m-1,n})}$$

$$e_{2m-1,n} = \frac{4\epsilon_{2m-1,n} (2m-1)(4m-3)(4m-1)}{[\epsilon_{2m-1,n}^2 - 16(2m-1)^2] J_{8m-4}^2(\epsilon_{2m-1,n})} \sum_{\mu=0}^{\infty} \frac{[8m+2\mu-3] J_{8m+2\mu-3}(\epsilon_{2m-1,n})}{(4m+\mu)(4m+\mu-1)(4m+\mu-3)(4m+\mu-2)}$$

and  $\epsilon_{2m-1,n}$  are the roots of  $J'_{8m-4}(\epsilon) = 0$ .

The pressure distribution at the webs,  $\varphi = 0$  and  $\varphi = \pi/4$ , is

$$(4.16) \quad p_{\text{WEB}} = \rho \Omega^2 a^2 \varphi_0 e^{i\Omega t} \left[ \mp \left( \frac{r}{a} \right)^2 \frac{\pi}{8} \pm \frac{2}{\pi^2} \sum_{m=1}^{\infty} \frac{\left[ \left( \frac{r}{a} \right)^{8m-4} - \frac{(\frac{r}{a})^2}{2(2m-1)} \right]}{(2m-1)[(2m-1)^2 - 1/4]} \right. \\ \left. \pm \frac{1}{\pi} \sum_{m=1}^{\infty} \sum_{n=0}^{\infty} \frac{\left[ \frac{f_{2m-1,n}}{2(2m-1)} + e_{2m-1,n} \right] J_{8m-4}(\epsilon_{2m-1,n} \frac{r}{a}) \eta_{2m-1,n}^2 \cosh[\epsilon_{2m-1,n} (\frac{z}{a} + \frac{h}{a})]}{[(2m-1)^2 - \frac{1}{4}] (1 - \eta_{2m-1,n}^2) \cosh(\epsilon_{2m-1,n} \frac{h}{a})} \right] - \rho g z$$

where the upper sign refers to the pressure at the web  $\varphi = 0$  and the lower sign to that of the web  $\varphi = \frac{\pi}{4}$ .

The pressure distribution at the container bottom is given by

$$(4.17) \quad p_{\text{bottom}} = \rho \Omega^2 a^2 \varphi_0 e^{i\Omega t} \left[ \left( \frac{r}{a} \right)^2 \left( \varphi - \frac{\pi}{8} \right) + \frac{2}{\pi} \sum_{m=1}^{\infty} \frac{\cos(8m-4)\varphi}{(2m-1)^2 \left[ (2m-1)^2 - \frac{1}{4} \right]} \left[ \left( \frac{r}{a} \right)^{8m-4} - \frac{\left( \frac{r}{a} \right)^2}{2(2m-1)} \right] + \frac{1}{\pi} \sum_{m=1}^{\infty} \sum_{n=0}^{\infty} \frac{\left[ \frac{r^{2m-1,n}}{2(2m-1)} - e_{2m-1,n} \right] J_{8m-4} \left( \epsilon_{2m-1,n} \frac{r}{a} \right) \eta_{2m-1,n}^2 \cos(8m-4)\varphi}{(1 - \eta_{2m-1,n}^2) \cosh \left( \epsilon_{2m-1,n} \frac{h}{a} \right) \left[ (2m-1)^2 - \frac{1}{4} \right]} \right] + \rho g h$$

#### 4.2. Pressure Distributions in Multi-Cell Tank of Ten Cells.

For the multi-cell container of ten cells the vertex angle assumes the value  $\pi/5$ , i.e. the value  $\alpha = 1/10$ . For free oscillations the pressure distribution at the tank wall is

$$(4.18) \quad p_{\text{wall}} = \rho \sum_{m=0}^{\infty} \sum_{n=0}^{\infty} \omega_{mn} [A_{mn} \sin(\omega_{mn} t) - B_{mn} \cos(\omega_{mn} t)] \frac{\cosh \left[ \epsilon_{mn} \left( \frac{z}{a} + \frac{h}{a} \right) \right]}{\cosh \left[ \epsilon_{mn} \frac{h}{a} \right]} J_{5m}(\epsilon_{mn}) \cdot \cos 5m\varphi - \rho g z$$

where the  $\epsilon_{mn}$ 's are the zeros of  $J_{5m}'(\epsilon) = 0$  and are presented in Table 2 for  $m = 0, 1, 2, 3, 4$ .

At the webs the pressure distributions are

$$(4.19) \quad p_{\text{web}}_{\varphi=0} = \rho \sum_{m=0}^{\infty} \sum_{n=0}^{\infty} \omega_{mn} [A_{mn} \sin(\omega_{mn} t) - B_{mn} \cos(\omega_{mn} t)] \frac{\cosh \left[ \epsilon_{mn} \left( \frac{z}{a} + \frac{h}{a} \right) \right]}{\cosh \left( \epsilon_{mn} \frac{h}{a} \right)} J_{5m} \left( \epsilon_{mn} \frac{r}{a} \right) - \rho g z$$

$$(4.20) \quad p_{\text{web}}_{\varphi=\frac{\pi}{5}} = \rho \sum_{m=0}^{\infty} \sum_{n=0}^{\infty} (-1)^n \omega_{mn} [A_{mn} \sin(\omega_{mn} t) - B_{mn} \cos(\omega_{mn} t)] \frac{\cosh \left[ \epsilon_{mn} \left( \frac{z}{a} + \frac{h}{a} \right) \right]}{\cosh \left( \epsilon_{mn} \frac{h}{a} \right)} J_{5m} \left( \epsilon_{mn} \frac{r}{a} \right) - \rho g z$$

At the bottom of the container the pressure distribution  $z = -h$  is given by

$$(4.21) \quad p_{\text{bottom}} = \rho \sum_{m=0}^{\infty} \sum_{n=0}^{\infty} \omega_{mn} [A_{mn} \sin(\omega_{mn} t) - B_{mn} \cos(\omega_{mn} t)] \frac{J_{5m}(\epsilon_{mn} \frac{r}{a})}{\cosh(\epsilon_{mn} \frac{h}{a})} \cos 5m\varphi \\ + \rho gh$$

For translational excitation with

$$(4.22) \quad a_0 = \frac{2.9389}{\pi} ; \quad c_0 = \frac{0.9549}{\pi} \\ a_m = \frac{(-1)^{m+1} 0.2351}{\pi [m^2 - 0.04]} ; \quad c_m = \frac{[(-1)^m \cdot 0.8090 - 1]}{\pi [m^2 - 0.04]} \cdot 0.4$$

$$(4.23) \quad b_{mn} = \frac{4a \epsilon_{mn} (25m^2 - 1)}{(\epsilon_{mn}^2 - 25m^2) J_{5m}^2(\epsilon_{mn})} \sum_{\mu=0}^{\infty} \frac{J_{5m+2\mu+1}(\epsilon_{mn})}{(5m+2\mu+3)(5m+2\mu-1)}$$

the pressure distribution at the wall  $r = a$  is

$$(4.24) \quad p_{\text{wall}} = \rho \Omega^2 e^{i\Omega t} \left[ \begin{array}{c} x_0 a \cos \varphi \\ y_0 a \sin \varphi \end{array} \right] \\ + \sum_{m=0}^{\infty} \sum_{n=0}^{\infty} \frac{\left[ \begin{array}{c} x_0 a \\ y_0 a \end{array} \right] b_{mn} J_{5m}(\epsilon_{mn}) \eta_{mn}^2 \cosh(\epsilon_{mn} (\frac{z}{a} + \frac{h}{a}))}{(1 - \eta_{mn}^2) \cosh(\epsilon_{mn} \frac{h}{a})} \cos 5m\varphi \Big] - \rho gz.$$

At the webs the pressure distribution yields

$$(4.25) \quad p_{web \varphi=0} = \rho \Omega^2 e^{i\Omega t} \left[ \begin{bmatrix} x_o r \\ 0 \end{bmatrix} + \sum_{m=0}^{\infty} \sum_{n=0}^{\infty} \frac{\begin{bmatrix} x_o a_m \\ y_o c_m \end{bmatrix} b_{mn} J_{5m} \left( \epsilon_{mn} \frac{r}{a} \right) \eta_{mn}^2 \cosh \left[ \epsilon_{mn} \left( \frac{z}{a} + \frac{h}{a} \right) \right]}{(1 - \eta_{mn}^2) \cosh \left( \epsilon_{mn} \frac{h}{a} \right)} \right] - \rho g z$$

and

$$(4.26) \quad p_{web \varphi = \pi/5} = \rho \Omega^2 e^{i\Omega t} \left[ \begin{bmatrix} x_o r \cos \varphi \\ y_o r \sin \varphi \end{bmatrix} + \sum_{m=0}^{\infty} \sum_{n=0}^{\infty} \frac{\begin{bmatrix} a_m x_o \\ c_m y_o \end{bmatrix} b_{mn} J_{5m} \left( \epsilon_{mn} \frac{r}{a} \right) \eta_{mn}^2 (-1)^m \cosh \left( \epsilon_{mn} \left( \frac{h}{a} + \frac{z}{a} \right) \right)}{(1 - \eta_{mn}^2) \cosh \left( \epsilon_{mn} \frac{h}{a} \right)} \right] - \rho g z$$

The pressure distribution at the container bottom is given by the expression

$$(4.27) \quad p_{Bottom} = \rho \Omega^2 e^{i\Omega t} \left[ \begin{bmatrix} x_o r \cos \varphi \\ y_o r \sin \varphi \end{bmatrix} + \sum_{m=0}^{\infty} \sum_{n=0}^{\infty} \frac{\begin{bmatrix} a_m x_o \\ c_m y_o \end{bmatrix} b_{mn} J_{5m} \left( \epsilon_{mn} \frac{r}{a} \right) \eta_{mn}^2 \cos 5m\varphi}{(1 - \eta_{mn}^2) \cosh \left( \epsilon_{mn} \frac{h}{a} \right)} \right] + \rho g h$$

For pitching and yawing excitations the pressure distribution yields with the expressions  $C_{mn}$  and  $D_{mn}$  (2.17) the values

$$(4.28) \quad p_{\text{wall}} = -\rho\Omega^2 e^{i\Omega t} \left[ \begin{bmatrix} \theta_o^{az} \cos \varphi \\ \chi_o^{az} \sin \varphi \end{bmatrix} - \begin{bmatrix} \theta_o \\ \chi_o \end{bmatrix} \sum_{m=0}^{\infty} \sum_{n=0}^{\infty} \left[ C_{mn} \cosh \left( \epsilon_{mn} \frac{z}{a} \right) + D_{mn} \sinh \left( \epsilon_{mn} \frac{z}{a} \right) \right] \cdot J_{5m}(\epsilon_{mn}) \cos 5m\varphi \right] - \rho g \left( z - \frac{h}{2} \right)$$

At the webs the pressure distribution is

$$(4.29) \quad p_{\text{web } \varphi=0} = -\rho\Omega^2 e^{i\Omega t} \left\{ \begin{bmatrix} \theta_o^{rz} \\ 0 \end{bmatrix} - \begin{bmatrix} \theta_o \\ \chi_o \end{bmatrix} \sum_{m=0}^{\infty} \sum_{n=0}^{\infty} \left[ C_{mn} \cosh \left( \epsilon_{mn} \frac{z}{a} \right) + D_{mn} \sinh \left( \epsilon_{mn} \frac{z}{a} \right) \right] \cdot J_{5m}(\epsilon_{mn}) \right\} - \rho g \left( z - \frac{h}{2} \right)$$

and

$$(4.30) \quad p_{\text{web } \varphi=\pi/5} = -\rho\Omega^2 e^{i\Omega t} \left\{ \begin{bmatrix} \theta_o^{rz} \cos \pi/5 \\ \chi_o^{rz} \sin \pi/5 \end{bmatrix} - \begin{bmatrix} \theta_o \\ \chi_o \end{bmatrix} \sum_{m=0}^{\infty} \sum_{n=0}^{\infty} \left[ C_{mn} \cosh \left( \epsilon_{mn} \frac{z}{a} \right) + D_{mn} \sinh \left( \epsilon_{mn} \frac{z}{a} \right) \right] \cdot (-1)^m J_{5m} \left( \epsilon_{mn} \frac{r}{a} \right) \right\} - \rho g \left( z - \frac{h}{2} \right)$$

At the container bottom it is

$$(4.31) \quad p_{\text{Bottom}} = -\rho\Omega^2 e^{i\Omega t} \left\{ \begin{aligned} & \left[ \begin{aligned} & -\theta_o r \frac{h}{2} \cos \varphi \\ & -\chi_o r \frac{h}{2} \sin \varphi \end{aligned} \right] - \left[ \begin{aligned} & \theta_o \\ & \chi_o \end{aligned} \right] \sum_{m=0}^{\infty} \sum_{n=0}^{\infty} \left[ C_{mn} \cosh \left( \frac{\epsilon_{mn}}{2} \frac{h}{a} \right) \right. \\ & \left. - D_{mn} \sinh \left( \frac{\epsilon_{mn}}{2} \frac{h}{a} \right) \right] \cdot J_{5m} \left( \epsilon_{mn} \frac{r}{a} \right) \cos 5m\varphi \end{aligned} \right\} + \rho gh.$$

For roll excitation the pressure distribution at the cylindrical wall is given by

$$(4.32) \quad p_{\text{wall}} = \rho\Omega^2 a^2 \varphi_o e^{i\Omega t} \left[ \left( \varphi - \frac{\pi}{10} \right) + \frac{8}{\pi^2} \sum_{m=1}^{\infty} \frac{\cos [5(2m-1)\varphi]}{(2m-1)^2 (10m-3)} + \frac{20}{\pi} \sum_{m=1}^{\infty} \sum_{n=0}^{\infty} \right. \\ \left. \frac{\left[ \frac{2}{5(2m-1)} f_{2m-1,n} e_{2m-1,n} \right] J_{5(2m-1)}(\epsilon_{2m-1,n}) \eta_{2m-1,n}^2 \cosh \left[ \epsilon_{2m-1,n} \left( \frac{z}{a} + \frac{h}{a} \right) \right] \cos [5(2m-1)\varphi]}{[25(2m-1)^2 - 4] (1 - \eta_{2m-1,n}^2 \cosh (\epsilon_{2m-1,n} \frac{h}{a}))} \right] \\ - \rho gz$$

where the values  $f_{2m-1,n}$  and  $e_{2m-1,n}$  are given by

$$f_{2m-1,n} = \frac{10(2m-1)}{[\epsilon_{2m-1,n}^2 - 25(2m-1)^2] J_{5(2m-1)}(\epsilon_{2m-1,n})}$$

$$e_{2m-1,n} = \frac{20\epsilon_{2m-1,n}^{(2m-1)(10m-7)(10m-3)}}{[\epsilon_{2m-1,n}^2 - 25(2m-1)^2] J_{10m-5}^2(\epsilon_{2m-1,n})} \sum_{\mu=0}^{\infty}$$

$$\frac{(10m + 2\mu - 4) J_{10m+2\mu-4}(\epsilon_{2m-1,n})}{(10m + 2\mu - 7)(10m + 2\mu - 5)(10m + 2\mu - 3)(10m + 2\mu - 1)}$$

and the value  $\epsilon_{2m-1,n}$  are the roots of  $J'_{10m-5}(\epsilon) = 0$ . The pressure distribution at the webs  $\varphi = 0$  and  $\varphi = \pi/5$  is

$$\begin{aligned}
(4.33) \quad p_{web} = \rho \Omega^2 a^2 \varphi_0 e^{i\Omega t} \left\{ \mp \left(\frac{r}{a}\right)^2 \frac{\pi}{10} \pm \frac{40}{\pi^2} \sum_{m=1}^{\infty} \frac{\left[\left(\frac{r}{a}\right)^{5(2m-1)} - \frac{2}{5(2m-1)} \left(\frac{r}{a}\right)^2\right]}{(2m-1) [25(2m-1)^2 - 4]} \right. \\
\left. \pm \frac{20}{\pi} \sum_{m=1}^{\infty} \sum_{n=0}^{\infty} \frac{\left[\frac{2}{5(2m-1)} f_{2m-1,n} - e_{2m-1,n}\right] J_{5(2m-1)}\left(\epsilon_{2m-1,n} \frac{r}{a}\right) \eta_{2m-1,n}^2 \cosh}{[25(2m-1)^2 - 4](1 - \eta_{2m-1,n}^2) \cosh\left(\epsilon_{2m-1,n} \frac{h}{a}\right)} \right. \\
\left. \frac{[\epsilon_{2m-1,n} (\frac{z}{a} + \frac{h}{a})]}{[25(2m-1)^2 - 4]} \right\} - \rho g z
\end{aligned}$$

where the upper sign refers to the pressure of the web  $\varphi = 0$  and the lower sign to that of the web  $\varphi = \pi/5$ .

The pressure distribution of the container bottom is given by

$$\begin{aligned}
(4.34) \quad p_{bottom} = \rho \Omega^2 a^2 \varphi_0 e^{i\Omega t} \left[ \left(\frac{r}{a}\right)^2 \left(\varphi - \frac{\pi}{10}\right) \right. \\
\left. + \frac{40}{\pi^2} \sum_{m=1}^{\infty} \frac{\cos[5(2m-1)\varphi] \left[\left(\frac{r}{a}\right)^{5(2m-1)} - \frac{2}{5(2m-1)} \left(\frac{r}{a}\right)^2\right]}{(2m-1) [25(2m-1)^2 - 4]} + \frac{20}{\pi} \sum_{m=1}^{\infty} \sum_{n=0}^{\infty} \right. \\
\left. \frac{\left[\frac{2}{5(2m-1)} f_{2m-1,n} - e_{2m-1,n}\right] J_{5(2m-1)}\left(\epsilon_{2m-1,n} \frac{r}{a}\right) \eta_{2m-1,n}^2 \cos[5(2m-1)\varphi]}{(1 - \eta_{2m-1,n}^2) \cosh\left(\epsilon_{2m-1,n} \frac{h}{a}\right) [25(2m-1)^2 - 4]} \right] + \rho g h
\end{aligned}$$

#### 4.3. Pressure Distributions in Multi-Cell Tank of Twelve Cells.

For a container of vertex angle  $\pi/6$ ,  $\alpha$  is assuming the value  $\alpha = 1/12$  and the pressure distributions for free oscillations are:

$$(4.35) \quad p_{\text{wall}} = \rho \sum_{m=0}^{\infty} \sum_{n=0}^{\infty} \omega_{mn} [A_{mn} \sin(\omega_{mn} t) - B_{mn} \cos(\omega_{mn} t)] \frac{\cosh[\epsilon_{mn} (\frac{z}{a} + \frac{h}{a})]}{\cosh(\epsilon_{mn} \frac{h}{a})} J_{6m}(\epsilon_{mn}) \cos(6m\varphi) - \rho g z$$

where the values  $\epsilon_{mn}$  are the zeros of  $J'_{6m}(\epsilon) = 0$  and are presented in Table 3.

At the webs the pressure distributions are

$$(4.36) \quad p_{\text{web } \varphi=0} = \rho \sum_{m=0}^{\infty} \sum_{n=0}^{\infty} \omega_{mn} [A_{mn} \sin(\omega_{mn} t) - B_{mn} \cos(\omega_{mn} t)] \frac{\cosh[\epsilon_{mn} (\frac{z}{a} + \frac{h}{a})]}{\cosh(\epsilon_{mn} \frac{h}{a})} J_{6m}(\epsilon_{mn} \frac{r}{a}) - \rho g z$$

$$(4.37) \quad p_{\text{web } \varphi=\pi/6} = \rho \sum_{m=0}^{\infty} \sum_{n=0}^{\infty} (-1)^m \omega_{mn} [A_{mn} \sin(\omega_{mn} t) - B_{mn} \cos(\omega_{mn} t)] \frac{\cosh[\epsilon_{mn} (\frac{z}{a} + \frac{h}{a})]}{\cosh(\epsilon_{mn} \frac{h}{a})} J_{6m}(\epsilon_{mn} \frac{r}{a}) - \rho g z$$

The pressure distribution at the container bottom is

$$(4.38) \quad p_{\text{bottom}} = \rho \sum_{m=0}^{\infty} \sum_{n=0}^{\infty} \omega_{mn} [A_{mn} \sin(\omega_{mn} t) - B_{mn} \cos(\omega_{mn} t)] \frac{J_{6m}(\epsilon_{mn} \frac{r}{a})}{\cosh(\epsilon_{mn} \frac{h}{a})} \cos(6m\varphi) + \rho g h$$

For translational excitation with

$$(4.39) \quad a_o = \frac{3}{\pi} \quad c_o = \frac{3(2\sqrt{3})}{\pi}$$

$$a_m = \frac{6(-1)^{m+1}}{\pi[36m^2-1]} \quad c_m = \frac{6[(-1)^m\sqrt{3}-1]}{\pi[36m^2-1]}$$

$$(4.40) \quad b_{mn} = \frac{4a(36m^2-1)\epsilon_{mn}}{[\epsilon_{mn}^2 - 36m^2] J_{6m}^2(\epsilon_{mn})} \sum_{\mu=0}^{\infty} \frac{J_{6m+2\mu+1}(\epsilon_{mn})}{(6m+2\mu+3)(6m+2\mu-1)}$$

the pressure distribution at the cylindrical wall of the container is

$$(4.41) \quad p_{wall} = \rho\Omega^2 e^{i\Omega t} \left\{ \begin{bmatrix} x_o a \cos \varphi \\ y_o a \sin \varphi \end{bmatrix} + \sum_{m=0}^{\infty} \sum_{n=0}^{\infty} \frac{\begin{bmatrix} a_m x_o \\ c_m y_o \end{bmatrix} b_{mn} J_{6m}(\epsilon_{mn}) \eta_{mn}^2 \cosh[\epsilon_{mn}(\frac{z}{a} + \frac{h}{a})]}{(1 - \eta_{mn}^2) \cosh(\epsilon_{mn} \frac{h}{a})} \cdot \cos(6m\varphi) \right\} - \rho g z$$

At the webs the pressure distribution yields

$$(4.42) \quad p_{web \varphi=0} = \rho\Omega^2 e^{i\Omega t} \left\{ \begin{bmatrix} x_o r \\ 0 \end{bmatrix} + \sum_{m=0}^{\infty} \sum_{n=0}^{\infty} \frac{\begin{bmatrix} a_m x_o \\ b_m y_o \end{bmatrix} b_{mn} J_{6m}(\epsilon_{mn} \frac{r}{a}) \eta_{mn}^2 \cosh[\epsilon_{mn}(\frac{z}{a} + \frac{h}{a})]}{(1 - \eta_{mn}^2) \cosh(\epsilon_{mn} \frac{h}{a})} \right\} - \rho g z$$

and

$$(4.43) \quad p_{web} \varphi=\pi/6 = \rho \Omega^2 e^{i\Omega t} \left\{ \begin{bmatrix} x_o^r \cos \pi/6 \\ y_o^r \sin \pi/6 \end{bmatrix} + \sum_{m=0}^{\infty} \sum_{n=0}^{\infty} \frac{\begin{bmatrix} a_m x_o \\ b_m y_o \end{bmatrix} b_{mn} (-1)^m J_{6m}(\epsilon_{mn} \frac{r}{a}) \eta_{mn}^2 \cosh [\epsilon_{mn} (\frac{z}{a} + \frac{h}{a})]}{(1 - \eta_{mn}^2) \cosh (\epsilon_{mn} \frac{h}{a})} \right\} - \rho g z$$

At the container bottom the pressure distribution is

$$(4.44) \quad p_{Bottom} = \rho \Omega^2 e^{i\Omega t} \left\{ \begin{bmatrix} x_o^r \cos \varphi \\ y_o^r \sin \varphi \end{bmatrix} + \sum_{m=0}^{\infty} \sum_{n=0}^{\infty} \frac{\begin{bmatrix} a_m x_o \\ b_m y_o \end{bmatrix} b_{mn} J_{6m}(\epsilon_{mn} \frac{r}{a}) \eta_{mn}^2 \cos (6m\varphi)}{(1 - \eta_{mn}^2) \cosh (\epsilon_{mn} \frac{h}{a})} \right\} + \rho g h$$

For pitching and yawing excitation the pressure distribution at the cylindrical wall of the tank is given by

$$(4.45) \quad p_{wall} = \rho \Omega^2 e^{i\Omega t} \left\{ \begin{bmatrix} \theta_o^{az} \cos \varphi \\ \chi_o^{az} \sin \varphi \end{bmatrix} - \begin{bmatrix} \theta_o \\ \chi_o \end{bmatrix} \sum_{m=0}^{\infty} \sum_{n=0}^{\infty} [C_{mn} \cosh (\epsilon_{mn} \frac{z}{a}) + D_{mn} \sinh (\epsilon_{mn} \frac{z}{a})] \cdot J_{6m}(\epsilon_{mn}) \cos (6m\varphi) \right\} - \rho g (z - \frac{h}{2})$$

where again the values  $C_{mn}$  and  $D_{mn}$  are given by the equations (2.17). For the appearing  $b_{mn}$  the expression (4.41) has to be introduced. The pressure distribution at the web,  $\varphi = 0$  and  $\varphi = \pi/6$ , is given by

$$(4.46) \quad p_{web \varphi=0} = \rho \Omega^2 e^{i\Omega t} \left\{ \begin{bmatrix} \theta_o r z \\ 0 \end{bmatrix} - \begin{bmatrix} \theta_o \\ \chi_o \end{bmatrix} \sum_{m=0}^{\infty} \sum_{n=0}^{\infty} [C_{mn} \cosh(\epsilon_{mn} \frac{z}{a}) + D_{mn} \sinh(\epsilon_{mn} \frac{z}{a})] \cdot J_{6m}(\epsilon_{mn} \frac{r}{a}) \right\} - \rho g (z - \frac{h}{2})$$

and

$$(4.47) \quad p_{web \varphi=\pi/6} = - \rho \Omega^2 e^{i\Omega t} \left\{ \begin{bmatrix} \theta_o r z \cos \frac{\pi}{6} \\ \chi_o r z \sin \frac{\pi}{6} \end{bmatrix} - \begin{bmatrix} \theta_o \\ \chi_o \end{bmatrix} \sum_{m=0}^{\infty} \sum_{n=0}^{\infty} [C_{mn} \cosh(\epsilon_{mn} \frac{z}{a}) - D_{mn} \sinh(\epsilon_{mn} \frac{z}{a})] (-1)^m \cdot J_{6m}(\epsilon_{mn} \frac{r}{a}) \right\} - \rho g (z - \frac{h}{2})$$

At the container bottom it is

$$(4.48) \quad p_{bottom} = - \rho \Omega^2 e^{i\Omega t} \left\{ \begin{bmatrix} -\theta_o r \frac{h}{2} \cos \varphi \\ -\chi_o r \frac{h}{2} \sin \varphi \end{bmatrix} - \begin{bmatrix} \theta_o \\ \chi_o \end{bmatrix} \sum_{m=0}^{\infty} \sum_{n=0}^{\infty} [C_{mn} \cosh(\frac{\epsilon_{mn}}{2} \frac{h}{a}) - D_{mn} \sinh(\frac{\epsilon_{mn}}{2} \frac{h}{a})] \cdot J_{6m}(\epsilon_{mn} \frac{r}{a}) \cos(6m\varphi) \right\}$$

For roll excitation the pressure distribution at the cylindrical wall yields

$$(4.49) \quad p_{wall} = \rho \Omega^2 a^2 \varphi_o e^{i\Omega t} \left\{ \left( \varphi - \frac{\pi}{12} \right) + \frac{4}{\pi^2} \sum_{m=1}^{\infty} \frac{\cos[6(2m-1)\varphi]}{(2m-1)^2 [3(2m-1) + 1]} + \frac{6}{\pi} \sum_{m=1}^{\infty} \sum_{n=0}^{\infty} \frac{\left[ \frac{1}{3(2m-1)} f_{2m-1,n} - e_{2m-1,n} \right] J_{6(2m-1)}(\epsilon_{2m-1,n}) \eta_{2m-1,n}^2 \cosh[\epsilon_{2m-1,n} (\frac{z}{a} + \frac{h}{a})] \cos[6(2m-1)\varphi]}{[9(2m-1)^2 - 1] (1 - \eta_{2m-1,n}^2) \cosh(\epsilon_{2m-1,n} \frac{h}{a})} \right\} - \rho g z$$

where the values  $f_{2m-1,n}$  and  $e_{2m-1,n}$  are given by

$$f_{2m-1,n} = \frac{12(2m-1)}{[\epsilon_{2m-1,n}^2 - 36(2m-1)^2] J_{6(2m-1)}(\epsilon_{2m-1,n})}$$

and

$$e_{2m-1,n} = \frac{24\epsilon_{2m-1,n}(2m-1)(3m-2)(3m-1)}{[\epsilon_{2m-1,n}^2 - 36(2m-1)^2] J_{6(2m-1)}^2(\epsilon_{2m-1,n})} \sum_{\mu=0}^{\infty} \frac{[12m+2\mu-5] J_{12m+2\mu-5}(\epsilon_{2m-1,n})}{[6m+\mu-4](6m+\mu-3)(6m+\mu-2)(6m+\mu-1)}$$

The pressure distribution at the webs  $\varphi = 0$  and  $\varphi = \pi/6$  is

$$(4.50) \quad p_{web} = \rho \Omega_a^2 \varphi_0 e^{i\Omega t} \left\{ \mp \left(\frac{r}{a}\right)^2 \frac{\pi}{12} \pm \frac{12}{\pi^2} \sum_{m=1}^{\infty} \frac{\left[\left(\frac{r}{a}\right)^{6(2m-1)} - \frac{1}{3(2m-1)} \left(\frac{r}{a}\right)^2\right]}{(2m-1) [9(2m-1)^2 - 1]} \pm \frac{6}{\pi} \sum_{m=1}^{\infty} \sum_{n=0}^{\infty} \frac{\left[\frac{1}{3(2m-1)} f_{2m-1,n} - e_{2m-1,n}\right] J_{6(2m-1)}(\epsilon_{2m-1,n} \frac{r}{a}) \eta_{2m-1,n}^2 \cosh[\epsilon_{2m-1,n} (\frac{z}{a} + \frac{h}{a})]}{[9(2m-1)^2 - 1] (1 - \eta_{2m-1,n}^2) \cosh(\epsilon_{2m-1,n} \frac{h}{a})} \right\} - \rho g z$$

where the upper sign refers to the pressure at the web  $\varphi = 0$  and the lower sign to the web wall  $\varphi = \pi/6$ . The pressure at the container bottom yields the expression

$$(4.51) \quad p_{bottom} = \rho \Omega_a^2 \varphi_0 e^{i\Omega t} \left\{ \left(\frac{r}{a}\right)^2 \left(\varphi - \frac{\pi}{12}\right) + \frac{12}{\pi^2} \sum_{m=0}^{\infty} \frac{\cos[6(2m-1)\varphi]}{(2m-1)[9(2m-1)^2 - 1]} \left[ \left(\frac{r}{a}\right)^{6(2m-1)} - \frac{1}{3(2m-1)} \left(\frac{r}{a}\right)^2 \right] \right. \\ \left. + \frac{6}{\pi} \sum_{m=1}^{\infty} \sum_{n=0}^{\infty} \frac{\left[\frac{1}{3(2m-1)} f_{2m-1,n} - e_{2m-1,n}\right] J_{6(2m-1)}(\epsilon_{2m-1,n} \frac{r}{a}) \eta_{2m-1,n}^2 \cos[6(2m-1)\varphi]}{(1 - \eta_{2m-1,n}^2) \cosh(\epsilon_{2m-1,n} \frac{h}{a}) [9(2m-1)^2 - 1]} \right\} + \rho g h$$

TABLE 1  
ZEROS OF  $J'_{4m}(\epsilon_{mm}) = 0$

$m=0$	1	2	3	4	5	6
$n \backslash 0$	$4m=4$	$4m=8$	$4m=12$	$4m=16$	$4m=20$	$4m=24$
3.83171	5.31756	9.59581	13.82109	18.10419	22.26759	26.41110
7.01559	9.28240	14.11541	18.74485	23.26394	27.71172	32.10885
10.17347	12.68191	17.77401	22.62927	27.34733	31.97366	36.53336
13.32369	15.96411	21.22907	26.24604	31.11194	35.87393	40.55913
16.47063	19.19603	24.58720	29.72898	34.71248	39.58453	44.37289
19.61586	22.40103	27.88928	33.13145	38.21206	43.17654	48.05260
22.76008	25.58976	31.15533	36.48055	41.64331	46.68717	51.63937
25.90367	28.76784	34.39663	39.79194	45.02543	50.13856	55.15787
29.04683	31.93854	37.62008	43.07549	48.37069	53.54503	58.62415
32.18968	35.10392	40.83018	46.33777	51.68742	56.91635	62.04927

TABLE 2  
ZEROS OF  $J'_{5m}(\epsilon_{mm}) = 0$

$m=0$	1	2	3	4	5
$n \backslash 0$	$5m=5$	$5m=10$	$5m=15$	$5m=20$	$5m=25$
3.83171	6.41565	11.71594	16.95879	22.26759	27.44454
7.01559	10.51932	16.44767	22.14194	27.71172	33.20179
10.17347	13.98706	20.22302	26.17774	31.97366	37.66484
13.32369	17.31279	23.76072	29.90658	35.87393	41.72057
16.47063	20.57549	27.18202	33.47845	39.58453	45.55917
19.61586	23.80357	30.53451	36.95417	43.17654	49.26009
22.76008	27.01030	33.84197	40.36510	46.68717	52.86538
25.90367	30.20284	37.11800	43.72963	50.13856	56.40029
29.04683	33.38544	40.37107	47.05946	53.54503	59.88125
32.18968	36.56077	43.60677	50.36251	56.91635	63.31966

TABLE 3

ZEROS OF  $J'_m(\epsilon_{mn}) = 0$ 

$m=0$		1	2	3	4
$n \backslash 0$		$\epsilon_{m=6}$	$\epsilon_{m=12}$	$\epsilon_{m=18}$	$\epsilon_{m=24}$
	3.83171	7.50132	13.82109	20.18882	26.41110
	7.01559	11.73427	18.74485	25.49518	32.10885
	10.17347	15.26802	22.62927	29.67010	36.53336
	13.32369	18.63738	26.24604	33.50392	40.55913
	16.47063	21.93169	39.72898	37.16041	44.37289
	19.61586	25.18391	33.13145	40.70680	48.05260
	22.76008	28.40847	36.48055	44.17813	51.63937
	25.90367	31.61787	39.79194	47.59513	55.15787
	29.04683	34.81339	43.07549	50.97113	58.62415
	32.18968	37.99964	46.33777	54.31522	62.04927

## 5. ESTIMATE OF ERROR

The actual size of the multi-cell container deviates slightly from that of the one treated in the analysis, and it is desirable to have an estimate of the difference of the dynamic pressure in a multi-cell container and that of an equivalent circular sector tank. A circular cylindrical sector container was preferred for the analytical investigation since this type of container could be analytically treated. This is due to the fact that the container walls are coordinate surfaces and permit the separation of the variables of the problem. Another point for preferring the geometry of the chosen container is the faster assessment of the effect of the various parameters involved. An analytical formula for the pressure distribution exhibits very lucidly the effect of parameters, which could not have been performed with a numerical high speed computer program.

In order to assess the error involved in this slight deviation of the geometry, a very extreme comparison is performed as follows. Two container configurations which can be analytically assessed are chosen for comparison. Existing experimental evidence indicates that the effect of propellant sloshing in other container geometries can be approximated by making the free fluid surface areas and liquid volumes equal. In the very extreme case here treated of a rectangular container as compared with the circular cylinder if the pressure difference is comparatively small, one can assume that it will be small for the sector and multi-cell tank. While in the latter configuration the radii of curvature deviates only slightly, those of the here treated case compare a tank with a finite radius of curvature  $a$  and the infinite radius of curvature of a rectangular container (Figure 3).

To perform this analysis the quiescent free fluid surface areas have to be made equal. For a circular cylinder tank of radius  $a$  the free fluid surface area is  $\pi a^2$ , while for a rectangular container of square cross section the free fluid surface area is given by  $b^2$ , where  $b$  is the width of one side wall. Therefore  $b$  has to be chosen to be  $b = a\sqrt{\pi}$ . The velocity potential of the rectangular container due to translatory excitation can be determined to be

$$\Psi(x, z, t) = x_0 \Omega \sin \Omega t \left[ \left( \frac{b}{2} - x \right) + \frac{4b}{\pi^2} \sum_{n=1}^{\infty} \frac{\eta_{2n-1}^2 \cosh\left[\frac{(2n-1)\pi(z+h)}{b}\right] \cos\left[\frac{(2n-1)\pi x}{b}\right]}{(1-\eta_{2n-1}^2)(2n-1)^2 \cosh\left[\frac{(2n-1)\pi h}{b}\right]} \right]$$

and the pressure distribution on the right wall  $x = b$  yields with  $b = a\sqrt{\pi}$

$$p_{x=b} = [-\rho g z - \rho \Psi_t]_{x=b} = -\rho g z + \rho x_0 \Omega^2 \cos \Omega t \left[ \frac{a\sqrt{\pi}}{2} + \frac{4a}{\pi^{3/2}} \sum_{n=1}^{\infty} \right]$$

$$\frac{\eta_{2n-1}^2 \cosh\left[\frac{(2n-1)\sqrt{\pi}(z+h)}{a}\right]}{(1 - \eta_{2n-1}^2 + 2i\gamma_{2n-1}\eta_{2n-1})(2n-1)^2 \cosh(2n-1)\sqrt{\pi} \frac{h}{a}} \Big]$$

The square of the natural circular frequencies is

$$\omega_n^2 = \frac{g\pi n}{b} \tanh\left(\frac{n\pi h}{b}\right) = \frac{g\sqrt{\pi}n}{a} \tanh\left(\frac{n\sqrt{\pi}h}{a}\right)$$

and  $\gamma_{2n-1}$  is the damping factor of the liquid.

For a cylindrical container with circular cross section the velocity potential is given by

$$\Phi(r, \varphi, z, t) = -x_0 \Omega a \sin \Omega t \cos \varphi \left[ \frac{r}{a} + 2 \sum_{n=1}^{\infty} \frac{J_1\left(\epsilon_n \frac{r}{a}\right) \eta_n^2 \cosh\left[\frac{\epsilon_n(z+h)}{a}\right]}{(\epsilon_n^2 - 1) J_1(\epsilon_n) (1 - \eta_n^2) \cosh(\epsilon_n \frac{h}{a})} \right]$$

The pressure distribution at the container wall  $r = a$  yields then the expression.

$$p_{\text{wall}} = x_0 \Omega^2 \rho a \cos \Omega t \cos \varphi \left\{ 1 + 2 \sum_{n=1}^{\infty} \frac{\cosh \left[ \frac{\epsilon_n}{a} (z+h) \right] \bar{\eta}_n^2}{(\epsilon_n^2 - 1) \cosh(\epsilon_n \frac{h}{a}) (1 - \bar{\eta}_n^2 + 2\gamma_n i \bar{\eta}_n)} \right\} - \rho g z$$

where  $\epsilon_n$  are the roots of the first derivative of the Bessel function of first kind and first order ( $J_1'(\epsilon_n) = 0$ ). The square of the circular natural frequencies is given by

$$\bar{\omega}_n^2 = \frac{g \epsilon_n}{a} \tanh \left( \frac{\epsilon_n h}{a} \right)$$

The difference in the pressure distribution of these two containers should indicate the seriousness of the difference in the container geometry. It is

$$p_{x=b} - p_{\text{wall}} = x_0 \rho \Omega^2 \cos \Omega t \left\{ \frac{a \sqrt{\pi}}{2} - a \cos \varphi + 2 \sum_{n=1}^{\infty} \left[ \frac{2a}{\pi^{3/2}} \frac{\eta_{2n-1}^2}{(1 - \eta_{2n-1}^2 + 2i\gamma_{2n-1} \eta_{2n-1})} \cdot \frac{\cosh \left[ \frac{(2n-1) \sqrt{\pi}}{a} (z+h) \right]}{\cosh \left[ \frac{(2n-1) \sqrt{\pi} h}{a} \right]} - \frac{\bar{\eta}_n^2 a \cos \varphi \cosh \left[ \frac{\epsilon_n}{a} (z+h) \right]}{(1 - \bar{\eta}_n^2 + 2i\gamma_n \bar{\eta}_n) (\epsilon_n^2 - 1) \cosh(\epsilon_n \frac{h}{a})} \right] \right\}$$

which has been evaluated for  $\frac{h}{a} = 4.0$ ,  $0 \leq \varphi \leq \pi/4$ , and various depths ( $-z$ ).

The natural frequencies  $f_{2n-1}$  of the rectangular container and those of the circular cylinder  $f_n$  agree quite well, as can be seen in Table 4.

TABLE 4

COMPARISON OF NATURAL FREQUENCIES OF CIRCULAR  
CYLINDRICAL CONTAINER AND RECTANGULAR TANK OF EQUAL SURFACE AREAS

n	$f_n / \sqrt{g/a}$	$f_{2n-1} / \sqrt{g/a}$
1	0.21595	0.21188
2	0.36748	0.36700
3	0.46500	0.47379
4	0.54453	0.56060
5	0.6136	0.63566
6	0.67553	0.70275
7	0.73218	0.76397
8	0.78473	0.82063
9	0.83397	0.87363
10	0.88042	0.92359

The numerical results for the pressure difference are presented in Figures 4 through 6. A damping of 4% critical is assumed to be present in the container. A container diameter of 2 meters was used in the numerical evaluation and the fluid height ratio was  $\frac{h}{a} = 4.0$ . The ratio of gravity to tank radius is then given by  $g/a = 10.0$ . With these values the pressure difference was determined versus forcing frequency for various depth locations ( $-z$ ) in the container and various angular positions  $\phi$ . For an excitation amplitude of 1/2 inch and a weight density of the liquid of 62.4 lb/ft<sup>3</sup> it is

$$p_{ax_0} = 0.24 \frac{\text{lbs sec}^2}{\text{ft}^2} = 0.00168 \frac{\text{lbs sec}^2}{(\text{inch})^2}$$

The pressure difference is therefore the indicated ordinate multiplied with the value  $\Omega^2$  and  $1.68 \cdot 10^{-3}$ . For instance for  $\varphi = 0$  near the first resonance  $\Omega^2 = 20 \text{ sec}^{-2}$  and the pressure difference at the free fluid surface is in the amount of  $(1/10)$  psi. This is a very conservative maximum value which will be smaller due to the breaking of the free fluid surface and a larger damping. Off resonance the pressure difference, of course, reduces drastically to values of about  $(1/100)$  psi and  $(1/300)$  psi. At a depth of  $0.2h$  under the fluid surface the maximum pressure difference is about  $0.04$  psi, while at half the depth it is about  $0.007$  psi. For  $\varphi = \pi/8$  and  $\pi/4$  the effects on the pressure difference are very similar except that the magnitude is slightly reduced.

From this very rough estimate of finite and infinite radius of curvature of the container wall it can be seen that in the case of a scalloped multi-cell container and the multi-cell container of circular sector cross section the pressure difference due to the slightly different container geometries is negligible, as long as the surface areas are made equal, i.e. as long as the radius of the sector container is chosen such that the cross-sectional areas of the container configurations are equal.

## 6. CONCLUSIONS

The pressure distribution along the circular container wall, the webs, and the container bottom has been given analytically for various excitation modes for a circular cylindrical sector container of vertex angle  $2\pi\alpha$ . Damping based on potential theory could be introduced into the results by expressing the values  $(1-\eta_{mn}^2)$  as  $(1-\eta_{mn}^2 + 2i\gamma_{mn}\eta_{mn})$ , where  $\gamma_{mn}$  is the damping factor of the  $(mn)$ th liquid mode and is obtained by experiments. The pressure distributions for various special tank configurations, such as the multi-cell container with 8, 10, 12 cells has been obtained and their analytical expressions are presented in section 4. Since the actual multi-cell container deviates slightly from the one treated here, an estimate of error in the pressure was performed for a rectangular and circular cylindrical container; it was found that even in this extreme case of finite and infinite radius of curvature of the container wall the error remains small for all practical purposes. The approximation of the scalloped tank with that of the multi-cell circular cylindrical sector container is therefore well justified. The pressure difference remains small (Figures 4, 5, 6) and the natural frequencies agree very well (Table 4).

The webs of the multi-cell container can be perforated for the purpose of pressure and propellant equalizations between the various cells. The amount of perforation and its hole diameter, however, have to be chosen in such a fashion that the liquid dynamic properties of the multi-cell construction are preserved. This means that the sloshing masses that are considerably reduced by the insertion of longitudinal walls in a circular cylindrical container and the natural frequencies which are increased for a multi-cell container are maintained. If the perforation has too large an area or if the hole size

is too large, the propellant would behave as in a conventional circular cylinder. It would exhibit the low natural frequencies and the large sloshing masses of a circular cylinder container, and the perforated webs would only increase the damping of the propellant, which indeed would be a costly damping from the standpoint of weight considerations. Results [9] pertaining to information about perforation and hole size are presented in Figure 7. The effect on the fundamental natural frequency of the amplitude of excitation, percent and hole diameter of perforation, and liquid density and viscosity are exhibited for a multi-cell container of eight cells. It has been found previously by many experimentors that a 23-25% opening will provide the best perforation. As to the size of the hole of the perforation, the results clearly exhibit that the diameter should be chosen at least smaller than

$$d < \frac{5^{2/3} \nu^{2/3} x_o^{2/3} \cdot 10^2}{a^{2/3} g^{1/3}} \quad (\text{i.e. } Re < 10^4)$$

which yields

$$d < 293 \nu^{2/3} a^{-2/3} g^{-1/3} x_o^{2/3}$$

where  $\nu = \frac{\eta}{\rho}$  is the viscosity,  $g$  the longitudinal acceleration,  $a$  the container radius and  $x_o$  the excitation amplitude.

Recommendation: It is recommended that the numerical evaluation for various oriented container configurations be performed for at least the multi-cell container with ten cells. Nomogram type of presentations for natural frequencies and pressure distributions should be worked out to assist the designer with a fast reference for evaluation. The results, furthermore, should be correlated with the anticipated experimental results of a ten cell container at the Marshall Space Flight Center, NASA.

## 7. REFERENCES

1. Oberth, H., "Wege zur Raumschiffahrt," Oldenburg, München, Germany (1929), Chapter 7, pp 44-54.
2. Blumrich, J. F., "Multi-cell vs Cylindrical Booster," NASA, Marshall Space Flight Center, Internal Note IN-P&VE-SA-62-10, Huntsville, Alabama, (July 1962).
3. Blumrich, J. F., "Multi-cell Structures Studied for Large Boosters," Space/Aeronautics 39, pp 86-89 (January 1963).
4. Bauer, H. F., "Fluid Oscillations in the Containers of a Space Vehicle and Their Influence Upon Stability," NASA-TR-R-187 (1964).
5. Bauer, H.F., "Treibstoffschwingungen in Raketenbehältern und ihr Einfluss auf die Gesamtstabilität," Zeitschrift für Flugwissenschaften 12 (1964) Heft 3 und 6.
6. Bauer, H. F., "Liquid Sloshing in a Cylindrical Quartertank," AIAA Journal 1, No. 11 (November, 1963).
7. Bauer, H. F., "Liquid Sloshing in 45° Compartmented Sector Tank," AIAA Journal 2, No. 3 (March 1964).
8. Bauer, H.F., "Tables of Zeros of Cross Product Bessel Functions," Journal of Mathematics of Computation (January 1964).
9. Abramson, H. N., Chu, W. H., Garza, L. R., "Liquid Sloshing in 45° Sector Compartmented Cylindrical Tanks," Technical Report No. 3 (Contract NAS 8-1555) Southwest Research Institute, 1962.

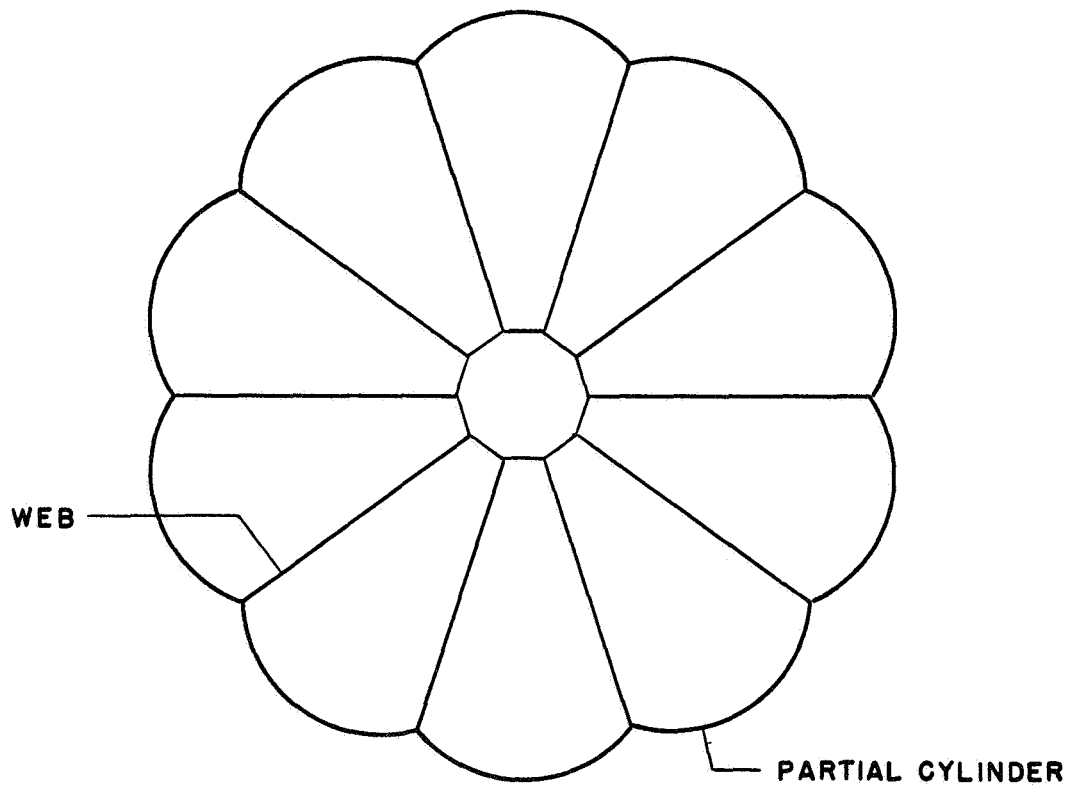


**FIGURE 1: CROSS SECTION OF MULTI-CELL CONTAINER**

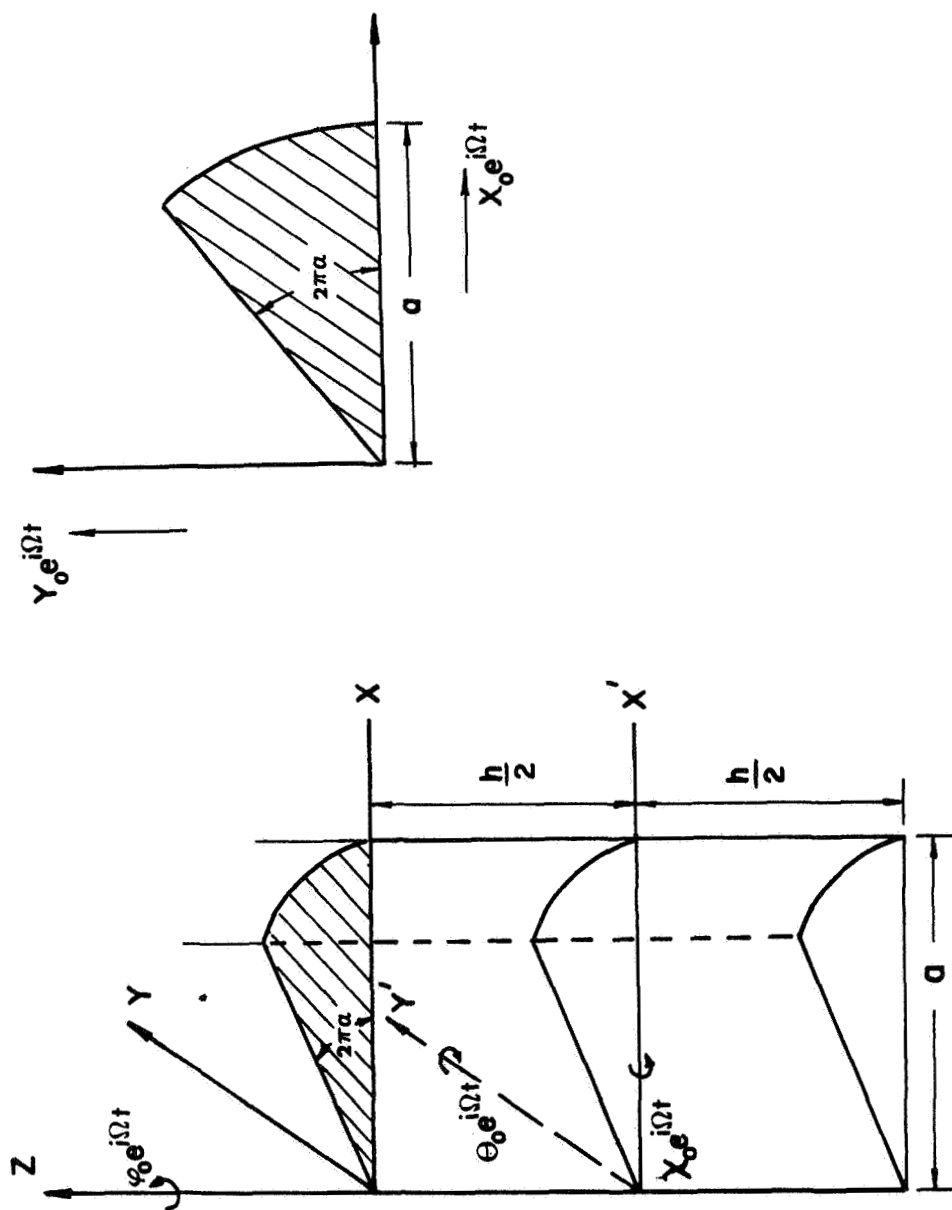
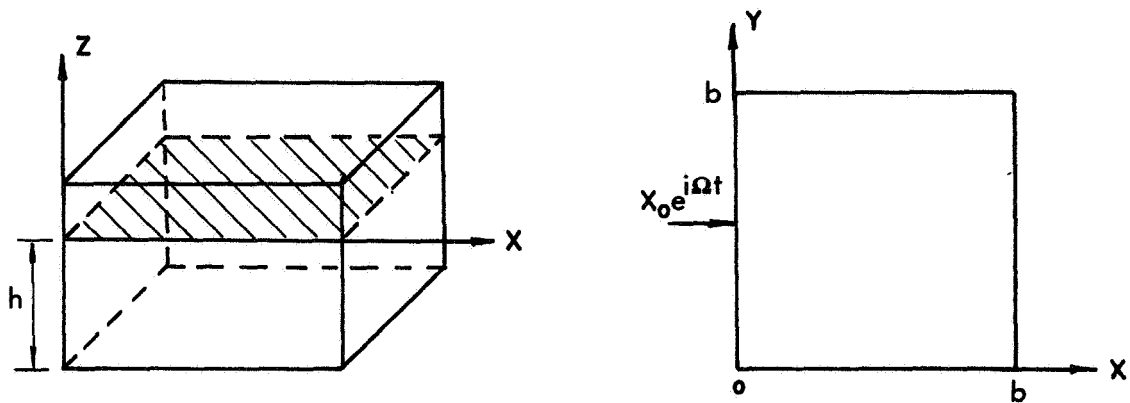
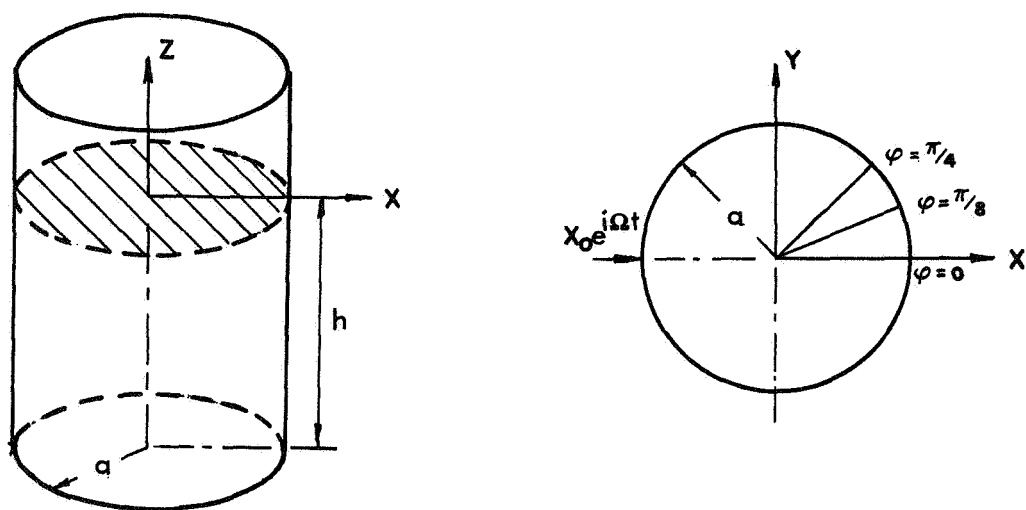


FIGURE 2: CIRCULAR CYLINDRICAL SECTOR TANK



RECTANGULAR CONTAINER



CIRCULAR CYLINDRICAL CONTAINER

FIGURE 3: COMPARISON OF RECTANGULAR AND CIRCULAR CONTAINERS

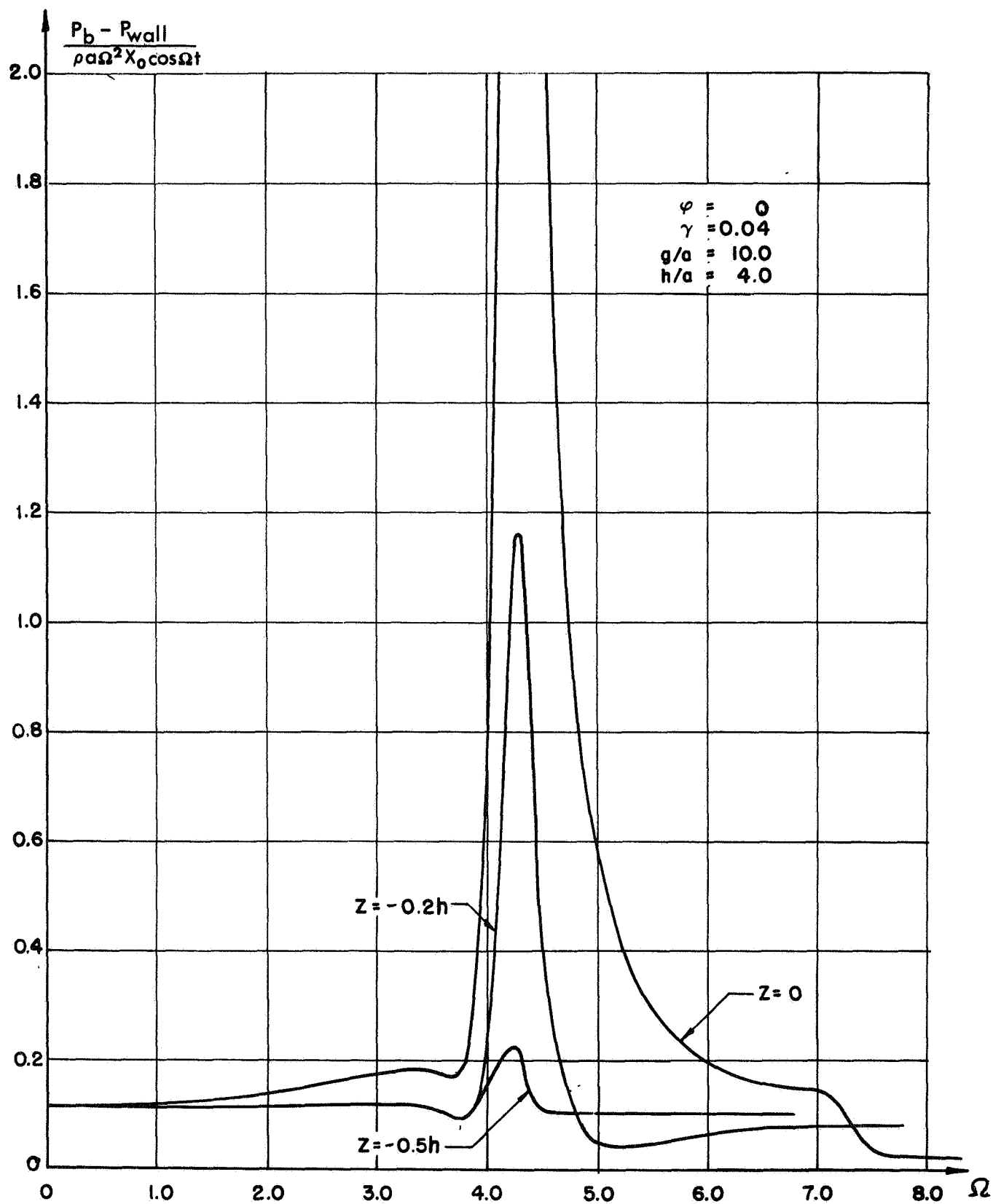


FIGURE 4: PRESSURE DIFFERENCE IN RECTANGULAR AND CIRCULAR CONTAINERS

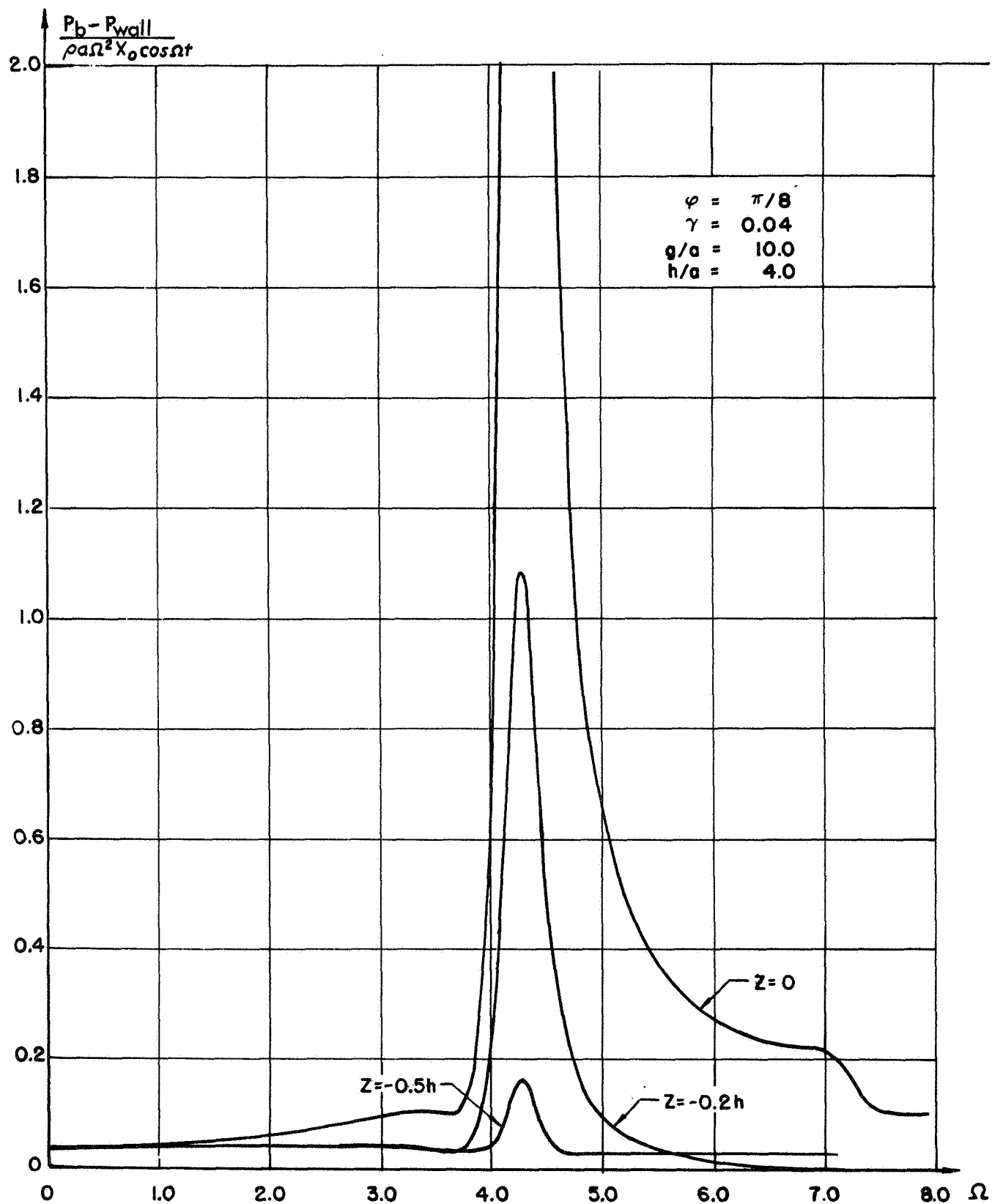


FIGURE 5: PRESSURE DIFFERENCE IN RECTANGULAR AND CIRCULAR CONTAINERS

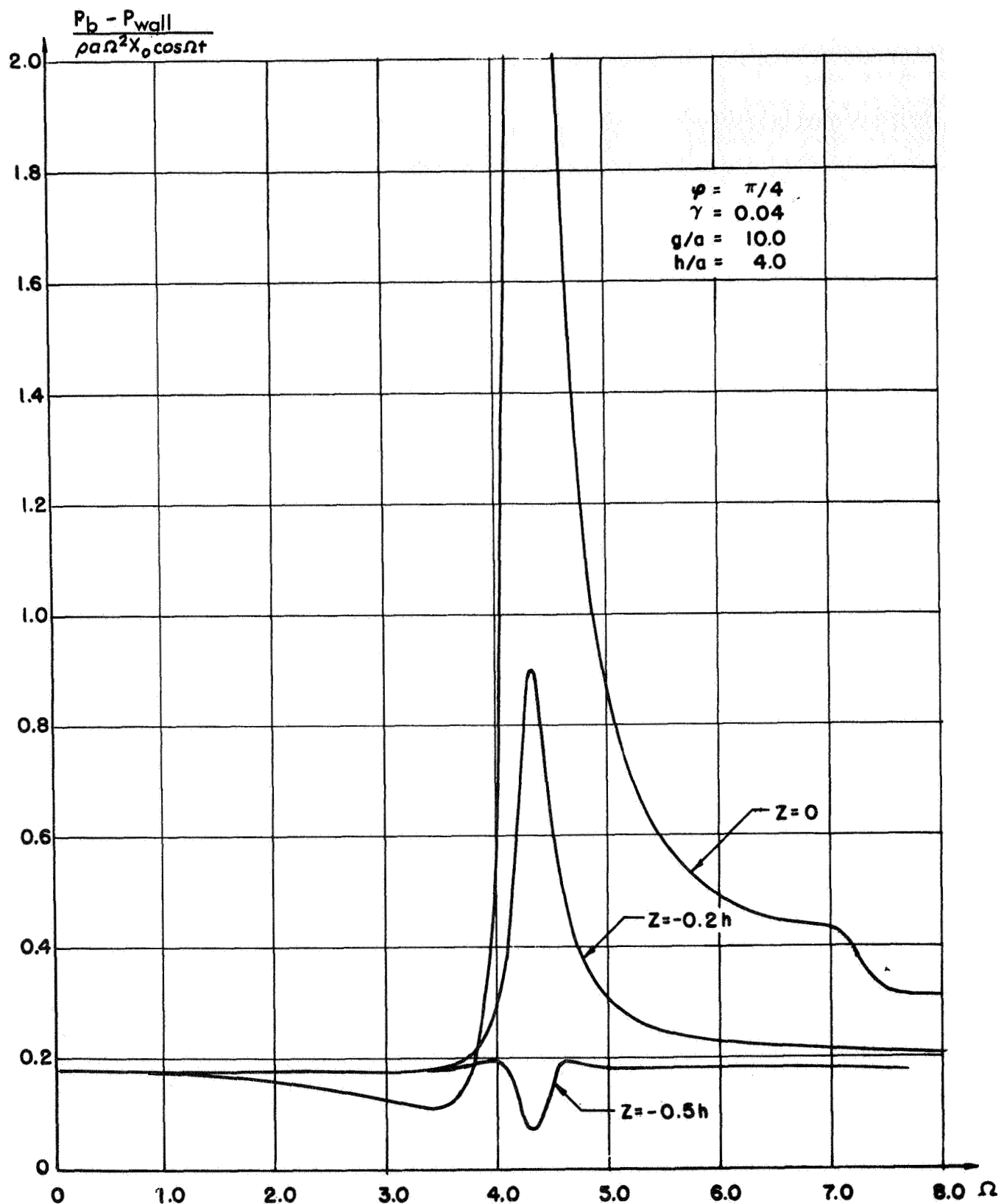


FIGURE 6: PRESSURE DIFFERENCE IN RECTANGULAR AND CIRCULAR CONTAINERS

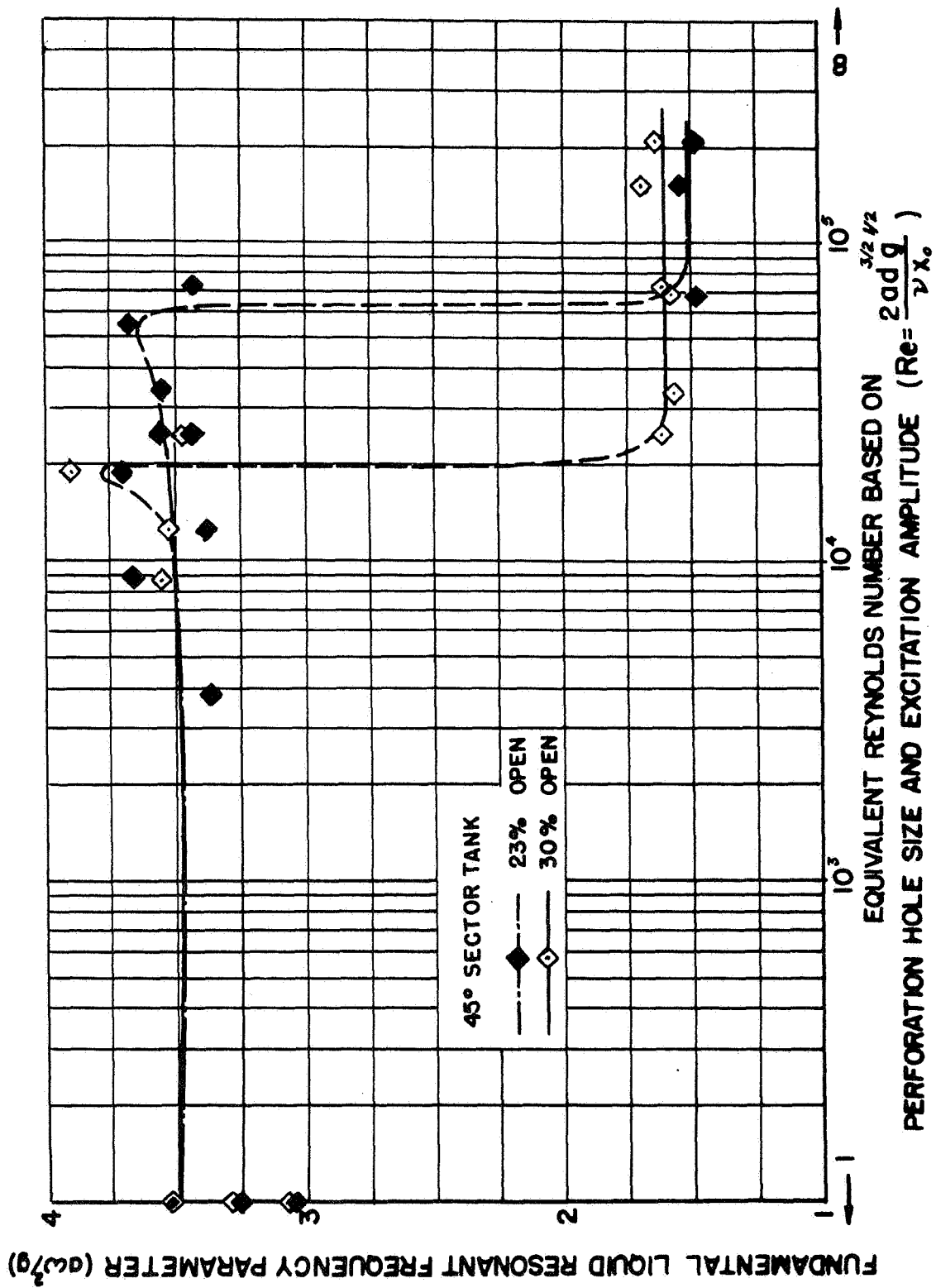


FIGURE 7: FUNDAMENTAL LIQUID FREQUENCY VERSUS EQUIVALENT REYNOLDS NUMBER